TABLE 1

General Characteristics of Sample Bursts.

Burst Name[a]	Trigger No.	Detector No.[b]	Model Used[c]	No. Spectra	Time Interval (s)	Average $E_{\rm peak}$ (keV)	Fluence ($erg\ cm^{-2}$)[d]
3B 910421	105	7	GRB	14	6.4e−2 − 10.3	127.3	8.2e−6
3B 910425	109	4	GRB	14	−16. − 53.2	401.6	4.8e−5
3B 910503	143	6	GRB	27	0.7 − 4.8	679.9	7.9e−5
3B 910522	219	456	BPL	51	110. −136.	190.4	3.5e−5
3B 910601	249	2	GRB	15	0.0 − 17.9	306.6	2.1e−5
3B 910619	394	1	GRB	34	0.0 − 44.5	331.6	4.1e−5
3B 910627	451	4	GRB	16	0.0 − 12.0	125.1	1.5e−5
3B 910717	543	4	GRB	10	0.0 − 6.1	225.8	8.3e−6
3B 910807	647	0	BPL	23	0.0 − 28.3	162.1	2.6e−5
3B 910814C	676	2	GRB	18	0.0 − 54.6	434.8	3.0e−5
3B 910814	678	2	BPL	37	0.0 − 29.4	444.8	7.8e−5
3B 911031	973	3	GRB	37	0.0 − 33.7	367.2	3.0e−5
3B 911118	1085	4	BPL	50	0.0 − 13.7	161.4	5.6e−5
3B 911126	1121	4	GRB	28	19. − 29.9	251.3	2.0e−5
3B 911127	1122	1	GRB	36	0.0 − 28.7	137.9	2.4e−5
3B 911202	1141	7	GRB	31	6.4e−2 − 17.9	354.2	4.2e−5
3B 911209	1157	1	GRB	18	0.1 − 23.4	218.3	1.8e−5
3B 920210	1385	5	BPL	35	0.0 − 48.8	291.5	4.1e−5
3B 920226	1440	3	GRB	16	10. − 17.9	301.6	1.3e−5
3B 920311	1473	5	GRB	51	3. − 23.2	448.2	8.3e−5
3B 920315	1484	3	BPL	8	0.0 − 20.1	174.8	5.7e−6
3B 920406	1541	2	GRB	14	67. − 95.2	223.2	1.1e−4
3B 920513	1606	3	GRB	28	12. −102.	206.7	5.8e−5
3B 920525	1625	4	GRB	35	4. − 19.7	447.3	6.4e−5
3B 920622	1663	4	GRB	60	0.0 − 24.4	509.8	1.0e−4
3B 920627	1676	S2	GRB	29	6.4e−2 − 38.1	236.7	2.4e−5
3B 920711	1695	7	GRB	29	0.0 − 39.2	348.7	1.1e−4
3B 920718	1709	7	GRB	13	0.1 − 5.1	192.2	9.9e−6
3B 920723	1721	3	BPL	32	6.4e−2 − 30.5	208.9	2.6e−5
3B 920902	1886	5	GRB	30	6.4e−2 − 14.6	472.2	4.5e−5
3B 921003	1974	2	GRB	21	0.0 − 9.5	56.5	1.3e−5
3B 921009	1983	2	GRB	54	6.4e−2 − 29.2	253.8	6.3e−5
3B 921015	1989	4	BPL	31	110. −350.	128.1	4.4e−5
3B 921022	1997	2	GRB	22	0.0 − 45.8	66.1	2.0e−5
3B 921118	2061	4	BPL	16	0.0 − 50.6	250.6	2.2e−5
3B 921123	2067	1	GRB	44	12. − 31.7	243.7	5.7e−5
3B 921207	2083	0	GRB	36	0.0 − 14.3	202.3	4.9e−5
3B 921209	2090	1	GRB	17	0.0 − 13.9	183.0	1.2e−5
3B 921230	2110	57	BPL	29	−2. − 31.8	289.7	2.5e−5
3B 930106	2122	6	GRB	12	6.4e−2 − 73.9	137.4	1.9e−5
3B 930120	2138	0	GRB	13	68. −105.	138.8	3.7e−5
3B 930201	2156	1	BPL	39	9. −175.	161.9	1.2e−4
3B 930405	2286	6	GRB	26	0.0 − 25.2	238.1	2.4e−5
3B 930425	2316	1	GRB	33	0.0 − 29.4	173.6	2.4e−5
3B 930506	2329	3	GRB	26	0.0 − 13.9	557.9	1.2e−4
3B 930916	2533	3	GRB	43	0.0 − 39.5	319.8	7.1e−5
3B 930922	2537	1	GRB	23	6.4e−2 − 4.9	97.0	1.6e−5

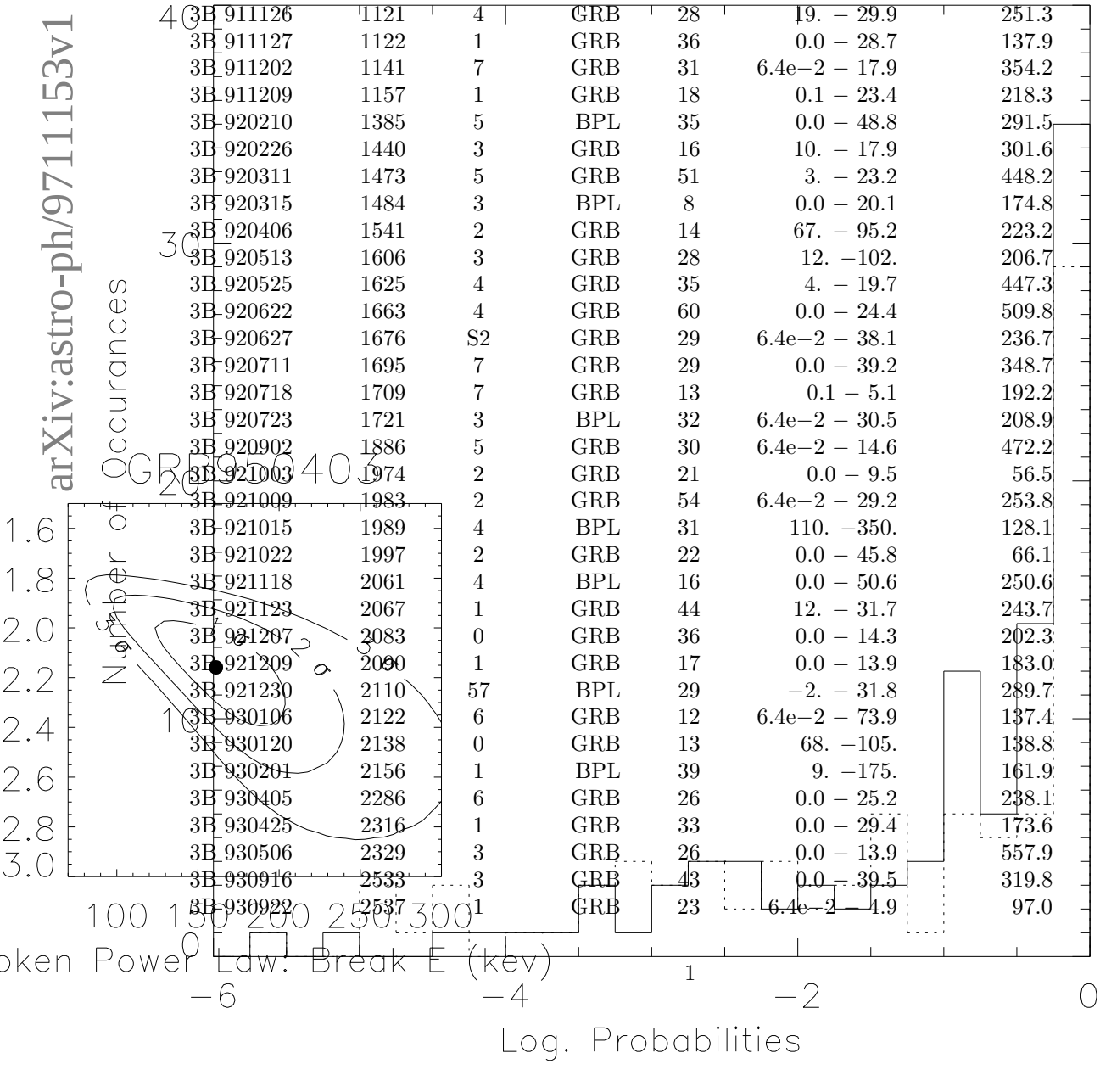

TABLE 1—*Continued*

Burst Name[a]	Trigger No.	Detector No.[b]	Model Used[c]	No. Spectra	Time Interval (s)	Average $E_{\rm peak}$ (keV)	Fluence ($erg\ cm^{-2}$)[d]
3B 931008	2571	236	BPL	43	3.0e−2 −164.	49.1	5.1e−5
3B 931026	2606	7	GRB	18	9. − 97.3	334.6	3.1e−5
3B 931103	2617	5	GRB	23	6.4e−2 − 18.7	430.1	2.5e−5
3B 931126	2661	1	GRB	18	0.0 − 12.9	160.8	2.9e−5
3B 931204	2676	1	GRB	59	0.0 − 15.8	336.3	8.1e−5
3B 940206	2798	13	BPL	65	3.0e−2 − 68.1	208.9	1.3e−4
3B 940210	2812	6	BPL	24	0.0 − 29.1	176.7	2.0e−5
3B 940217	2831	0	GRB	32	7. − 33.7	790.0	7.4e−5
3B 940228	2852	7	BPL	25	0.0 − 38.7	252.5	3.6e−5
3B 940301	2855	4	GRB	37	0.0 − 43.3	287.1	6.5e−5
3B 940302	2856	1	GRB	42	−3. −153.	308.8	2.2e−4
3B 940319	2889	4	GRB	10	6.4e−2 − 63.5	376.8	3.6e−5
3B 940323	2891	45	BPL	36	−2. − 24.4	470.3	4.3e−5
3B 940414	2929	4	GRB	36	0.0 − 46.2	710.0	4.6e−5
3B 940429	2953	3	GRB	33	0.0 − 25.1	165.0	2.7e−5
3B 940526B	2993	3	COMP	9	0.0 − 28.8	3031.0	2.1e−5
3B 940526	2994	1	BPL	44	3. − 27.3	509.5	5.0e−5
3B 940529	3003	0	GRB	13	0.0 − 35.6	279.6	1.9e−5
3B 940619	3035	6	GRB	13	0.0 − 62.0	200.6	1.9e−5
3B 940623	3042	1	GRB	19	0.1 − 16.2	342.1	1.5e−5
3B 940703	3057	S5	BPL	22	27. − 92.8	242.6	2.3e−4
3B 940708	3067	6	GRB	25	0.0 − 7.7	316.2	3.0e−5
3B 940810	3115	3	GRB	21	11. − 30.7	254.8	1.8e−5
3B 940817	3128	5	GRB	43	20. − 48.0	372.6	6.1e−5
3B 940826	3138	6	GRB	18	8. − 17.4	142.9	1.1e−5
4B 940921	3178	2	GRB	22	3.3e−2 − 24.8	662.0	5.4e−5
4B 941008	3227	5	GRB	14	82. − 93.1	253.0	1.2e−5
4B 941014	3241	6	GRB	37	19. − 44.7	360.6	3.0e−5
4B 941017	3245	4	GRB	91	5. − 86.6	317.5	1.6e−4
4B 941020	3253	S5	GRB	28	16. − 70.3	235.7	6.7e−5
4B 941023	3255	4	BPL	14	0.1 − 32.3	144.9	2.0e−5
4B 941121	3290	4	GRB	12	34. − 52.0	127.0	1.6e−5
4B 941228	3330	3	GRB	14	0.1 − 59.6	404.8	2.2e−5
4B 950104	3345	1	GRB	17	3.3e−2 − 11.6	226.8	1.4e−5
4B 950111	3352	2	GRB	28	3.3e−2 − 42.6	170.8	2.6e−5
4B 950208	3408	6	GRB	61	9.0e−2 − 28.3	410.2	5.5e−5
4B 950211	3415	5	GRB	25	2.6e−2 − 54.6	169.7	2.9e−5
4B 950301	3448	3	BPL	11	180. −338.	196.1	2.3e−5
4B 950305	3458	S4	GRB	17	3.3e−2 − 23.0	224.8	2.1e−5
4B 950325	3481	2	GRB	21	37. − 47.6	280.8	2.7e−5
4B 950401	3489	5	GRB	15	0.1 − 18.6	331.0	2.6e−5
4B 950403	3491	3	GRB	52	2. − 17.3	191.3	4.4e−5
4B 950403B	3492	5	GRB	26	3. − 9.0	406.9	4.3e−5
4B 950425	3523	6	BPL	58	3.3e−2 − 28.9	357.7	1.1e−4
4B 950513	3571	5	GRB	22	9.2e−2 − 36.4	282.4	2.3e−5
4B 950522	3593	2	BPL	14	2.6e−2 − 18.4	395.1	2.1e−5
4B 950701	3657	4	GRB	26	3.2e−2 − 9.6	256.6	2.3e−5

TABLE 1—*Continued*

Burst Name[a]	Trigger No.	Detector No.[b]	Model Used[c]	No. Spectra	Time Interval (s)	Average $E_{\rm peak}$ (keV)	Fluence ($erg\ cm^{-2}$)[d]
4B 950701B	3658	5	GRB	30	2.6e−2 − 11.4	233.8	2.0e−5
4B 950804	3734	4	GRB	15	0.1 − 3.7	311.0	2.0e−5
4B 950818	3765	1	GRB	31	52. − 73.3	255.3	3.4e−5
4B 950909	3788	3	GRB	23	1.5e−8 − 67.6	183.3	3.9e−5
4B 951011	3860	5	GRB	16	3.3e−2 − 29.8	516.7	2.9e−5
4B 951016	3870	5	GRB	16	2.6e−2 − 5.4	97.4	1.2e−5
4B 951102	3891	2	GRB	21	26. − 42.4	164.2	1.3e−5
4B 951203	3930	0	GRB	20	3.2e−2 − 21.1	546.8	5.4e−5
4B 951219	4039	6	COMP	19	2.5e−2 − 43.0	1301.8	3.7e−5
4B 960114	4368	S0	BPL	25	15. − 27.2	119.2	1.2e−4
4B 960124	4556	5	GRB	23	2.6e−2 − 5.0	251.4	1.6e−5
4B 960201	4701	1	GRB	21	7. − 26.3	227.2	2.1e−5
4B 960321	5299	S0	BPL	46	41. − 69.4	107.8	4.5e−5
4B 960322	5304	57	GRB	59	2.4e−2 − 26.9	278.3	7.3e−5
4B 960529	5477	1	COMP	20	9.1e−2 − 10.0	10423.7	3.5e−5
4B 960605	5486	23	BPL	46	60. − 89.4	220.9	5.9e−5
4B 960607	5489	1	GRB	26	30. − 55.0	280.6	2.9e−5
4B 960623	5512	5	BPL	13	3.3e−2 − 30.0	165.7	1.8e−5
4B 960807	5567	0	GRB	32	9.0e−2 − 17.8	300.2	2.7e−5
4B 960808	5568	6	GRB	8	0.2 − 5.6	513.3	1.9e−5
4B 960831	5591	67	BPL	49	−9. −167.	282.8	5.6e−5
4B 960924	5614	S6	BPL	27	7. − 13.1	201.2	1.5e−4
4B 961001	5621	2	GRB	25	2.6e−2 − 10.3	211.0	2.9e−5
4B 961009	5629	6	BPL	35	3.3e−2 − 15.9	189.8	2.1e−5
4B 961029	5649	15	GRB	59	4. −100.	239.4	1.7e−4
4B 961102	5654	15	GRB	63	3.0e−2 −100.	252.2	6.0e−5
4B 961202	5704	0	GRB	13	3.0e−2 − 5.2	127.0	1.2e−5
4B 970111	5773	0	COMP	57	2.9e−2 − 21.8	187.7	4.4e−5
4B 970202	5995	1	BPL	60	9.0e−2 − 21.6	265.8	7.3e−5
4B 970223	6100	6	BPL	35	9.0e−2 − 18.4	250.9	4.2e−5
4B 970306	6115	2	BPL	15	0.1 −108.	304.5	4.0e−5
4B 970315	6124	S2	BPL	47	2.6e−2 − 19.2	207.1	6.4e−5

[a]Burst names are from Meegan et al. 1996, and continue with a '4B' prefix for bursts that occurred after the end of the 3B Catalog.

[b]Entries with multiple detectors indicate that summed data were used for the analysis. Entries prefixed by 'S' indicate that SD data were used instead of missing LAD data.

[c]'GRB': the spectral form of Band et al. (1993); 'BPL': broken power law; and 'COMP': power law with a high−energy exponential cut−off, in the same $E_{\rm peak}$ parametrization as the GRB model.

[d]Fluences as determined over the selected time interval for the given spectral form; differs from the 3B Catalog values.

TABLE 2
Analysis of High Energy Spectral Index.

Burst Name[a]	$\beta_{\rm ave}$	χ^2 Probability:[b] Const. β	Linear β	Slope in β ($\times 10^{-2} s^{-1}$)	Correlations: Time	Intensity[c]	$E_{\rm peak}$
3B 910421	−2.36	5.3e−4	1.6e−2	−9.53±2.8	−0.534	2.3e−7	−0.231
3B 910425	−1.95	7.4e−1	9.3e−1	−1.14±0.6	−0.670	−1.4e−1	0.134
3B 910503	−2.10	2.8e−2	1.0e−1	−8.53±3.2	−0.332	5.1e−5	−0.167
3B 910522	−2.19	0.0	1.2e−7	−1.18±0.4	−0.249	5.4e−3	−0.389
3B 910601	−2.08	1.0e−1	5.0e−1	4.47±1.5	0.396	1.5e−1	−0.193
3B 910619	−1.72	2.0e−6	1.7e−2	−0.95±0.2	−0.339	3.0e−3	−0.318
3B 910627	−2.30	3.9e−5	8.2e−4	−3.40±1.1	−0.593	5.0e−9	0.579
3B 910717	−2.50	9.4e−1	9.4e−1	3.30±4.1	0.406	−3.0e−1	−0.491
3B 910807	−2.65	1.8e−4	1.3e−4	−0.39±0.5	0.143	3.0e−3	−0.411
3B 910814C	−1.66	1.8e−7	4.3e−1	−1.20±0.2	−0.664	−8.1e−5	−0.556
3B 910814	−1.65	1.2e−5	4.2e−2	−2.20±0.4	−0.729	−3.0e−2	−0.120
3B 911031	−1.91	5.1e−2	2.6e−1	−1.29±0.4	−0.711	4.6e−3	0.277
3B 911118	−2.61	0.0	3.0e−6	−7.30±0.4	−0.864	2.0e−3	0.709
3B 911126	−2.00	6.7e−1	9.2e−1	−5.97±2.4	−0.560	−6.3e−3	0.311
3B 911127	−2.26	2.6e−1	2.2e−1	0.03±0.5	−0.065	−5.5e−2	0.081
3B 911202	−1.99	8.2e−2	3.8e−1	−2.10±0.7	−0.453	−4.3e−2	−0.268
3B 911209	−2.03	2.9e−1	3.9e−1	−1.67±1.0	−0.088	1.0e−1	−0.055
3B 920210	−1.94	0.0	0.0	0.34±0.4	0.019	−6.7e−3	−0.413
3B 920226	−2.45	1.3e−1	5.0e−1	−12.12±4.6	−0.287	1.9e−3	−0.503
3B 920311	−2.23	0.0	3.5e−3	−4.51±0.5	−0.599	5.5e−8	0.338
3B 920315	−2.40	9.8e−4	1.3e−1	−31.69±8.3	−0.881	2.7e−1	−0.500
3B 920406	−2.32	1.5e−5	2.4e−3	−1.33±0.3	−0.723	9.9e−4	0.270
3B 920513	−2.44	9.1e−1	8.8e−1	0.08±0.2	−0.424	4.3e−3	0.088
3B 920525	−2.08	0.0	2.7e−1	−7.36±0.9	−0.814	2.4e−1	0.361
3B 920622	−2.01	9.5e−3	2.9e−2	1.03±0.4	−0.120	1.1e−5	−0.377
3B 920627	−1.84	5.3e−1	5.4e−1	0.35±0.3	−0.170	1.4e−3	0.226
3B 920711	−2.19	1.2e−4	1.4e−3	0.70±0.2	0.144	2.7e−3	−0.151
3B 920718	−2.62	9.1e−1	9.0e−1	−3.68±5.5	0.099	1.0e−1	−0.093
3B 920723	−2.47	0.0	0.0	−1.69±1.0	−0.100	−6.9e−6	−0.249
3B 920902	−2.04	9.5e−3	5.7e−2	−4.99±1.7	−0.574	1.5e−1	0.093
3B 921003	−3.45	0.0	2.1e−1	−19.59±2.3	−0.701	5.7e−2	0.625
3B 921009	−2.66	3.1e−1	6.2e−1	−1.40±0.5	−0.187	1.2e−1	−0.539
3B 921015	−2.31	0.0	0.0	0.12±0.0	−0.393	2.6e−3	−0.221
3B 921022	−1.99	0.0	0.0	−0.41±0.1	−0.294	−2.0e−1	−0.240
3B 921118	−1.98	4.0e−5	4.2e−5	−0.87±0.6	0.174	−3.9e−6	−0.315
3B 921123	−2.69	1.5e−1	1.4e−1	−0.62±0.8	−0.245	2.2e−5	−0.054
3B 921207	−2.96	3.3e−2	5.6e−1	−3.34±0.8	−0.331	7.0e−2	0.296
3B 921209	−2.34	5.9e−1	7.4e−1	−3.04±1.8	−0.335	−1.0e−1	0.288
3B 921230	−2.11	6.6e−7	4.2e−7	−0.49±0.8	−0.089	−6.4e−7	−0.806
3B 930106	−1.76	0.0	1.3e−3	0.72±0.1	0.601	−2.3e−1	−0.741
3B 930120	−2.43	8.0e−4	1.2e−1	1.61±0.4	0.336	2.2e−1	−0.536
3B 930201	−2.10	0.0	0.0	−0.32±0.0	−0.792	5.6e−5	0.338
3B 930405	−2.52	5.4e−2	6.1e−2	1.09±0.8	0.094	2.6e−2	0.019
3B 930425	−2.09	4.9e−1	4.3e−1	−0.08±0.5	−0.487	−4.4e−6	0.179
3B 930506	−1.69	0.0	0.0	−2.51±0.3	−0.596	7.3e−3	0.315
3B 930916	−1.94	6.0e−7	9.2e−6	0.87±0.3	0.166	−8.0e−5	−0.068
3B 930922	−2.58	5.2e−1	7.1e−1	−6.01±3.0	−0.447	4.2e−3	−0.060

TABLE 2—*Continued*

Burst Name[a]	$\beta_{\rm ave}$	χ^2 Probability:[b] Const. β	Linear β	Slope in β ($\times 10^{-2} s^{-1}$)	Correlations: Time	Intensity[c]	$E_{\rm peak}$
3B 931008	−1.57	0.0	0.0	−0.15±0.0	−0.396	1.6e−3	−0.226
3B 931026	−2.03	9.7e−1	9.5e−1	0.08±0.4	−0.063	−1.6e−2	−0.042
3B 931103	−2.12	4.6e−1	5.0e−1	−1.59±1.3	−0.098	1.2e−3	−0.346
3B 931126	−2.52	2.9e−3	1.8e−1	−6.51±1.7	−0.665	1.1e−1	0.456
3B 931204	−2.19	0.0	0.0	−5.88±0.6	−0.635	2.9e−2	−0.265
3B 940206	−2.12	0.0	0.0	−1.76±0.1	−0.550	2.0e−5	0.547
3B 940210	−2.14	2.4e−7	1.3e−1	−1.86±0.3	−0.565	−3.8e−2	−0.203
3B 940217	−2.22	1.0	1.0	−0.65±1.0	−0.241	2.8e−1	−0.084
3B 940228	−2.30	9.5e−4	7.3e−2	−1.41±0.3	−0.419	−3.4e−1	−0.254
3B 940301	−2.04	1.6e−2	3.7e−2	−0.65±0.3	−0.252	2.5e−1	0.018
3B 940302	−2.22	9.8e−1	9.9e−1	−0.16±0.1	−0.223	−7.0e−5	0.143
3B 940319	−2.13	7.4e−1	7.5e−1	−0.96±1.0	0.030	−9.3e−3	−0.127
3B 940323	−1.84	2.2e−3	9.7e−3	−1.51±0.6	−0.241	−3.2e−1	−0.616
3B 940414	−1.73	8.5e−1	8.3e−1	−0.24±0.3	0.087	−2.5e−1	−0.529
3B 940429	−2.04	0.0	0.0	−2.01±0.4	0.062	4.6e−4	0.181
3B 940526	−1.59	8.2e−3	2.2e−1	−2.90±0.7	−0.671	2.4e−2	−0.380
3B 940529	−1.77	2.0e−3	4.1e−1	−4.08±1.0	−0.891	−4.9e−2	0.564
3B 940619	−2.07	8.8e−1	8.6e−1	−0.25±0.4	−0.112	2.8e−1	0.091
3B 940623	−1.84	9.1e−1	9.1e−1	−1.53±1.8	−0.669	−1.4e−2	0.404
3B 940703	−1.78	0.0	0.0	−0.99±0.1	−0.694	8.0e−2	−0.007
3B 940708	−1.85	1.4e−3	6.8e−1	−8.00±1.5	−0.669	2.0e−1	0.093
3B 940810	−2.09	5.3e−3	7.6e−2	−4.38±1.3	−0.274	2.0e−1	0.223
3B 940817	−2.23	6.3e−1	9.5e−1	−1.60±0.5	−0.128	−5.8e−3	−0.288
3B 940826	−2.44	4.0e−4	2.9e−3	8.81±3.2	0.257	4.3e−2	−0.426
4B 940921	−1.78	2.8e−2	1.1e−1	−1.89±0.7	−0.411	9.5e−2	−0.215
4B 941008	−2.13	7.9e−1	8.6e−1	−3.39±2.6	−0.007	2.8e−1	−0.601
4B 941014	−2.12	9.5e−3	7.0e−1	−3.93±0.8	−0.657	6.8e−2	0.517
4B 941017	−2.26	0.0	2.7e−4	−0.97±0.1	−0.701	3.4e−8	0.520
4B 941020	−2.43	2.5e−1	5.2e−1	−0.70±0.3	−0.368	1.2e−2	−0.084
4B 941023	−2.57	0.0	1.0e−3	−2.98±0.4	−0.358	−3.9e−3	−0.103
4B 941121	−2.54	0.0	5.2e−4	−10.28±1.6	−0.804	3.8e−5	0.399
4B 941228	−1.78	1.4e−2	1.7e−1	−1.54±0.5	−0.681	9.3e−5	−0.374
4B 950104	−1.99	3.7e−1	3.4e−1	−1.46±2.0	0.169	−2.5e−2	0.022
4B 950111	−2.45	7.3e−1	6.7e−1	0.19±1.3	−0.126	−1.6e−5	0.728
4B 950208	−2.11	9.8e−1	1.0	−1.78±0.5	−0.566	2.0e−1	0.404
4B 950211	−2.23	1.5e−3	3.6e−2	−1.01±0.3	−0.149	3.2e−2	−0.106
4B 950301	−2.38	5.6e−1	4.8e−1	−0.13±0.4	−0.118	−2.3e−3	−0.827
4B 950305	−1.89	1.3e−1	1.4e−1	2.08±1.8	−0.015	−9.1e−3	0.038
4B 950325	−1.97	3.4e−3	8.3e−3	−3.83±1.8	−0.384	−4.9e−2	0.067
4B 950401	−2.50	8.6e−1	8.1e−1	−0.64±1.7	−0.028	3.5e−1	0.531
4B 950403	−2.25	0.0	4.8e−7	−7.16±0.4	−0.723	9.3e−7	0.511
4B 950403B	−2.22	8.9e−1	8.8e−1	−2.10±3.2	−0.072	2.5e−1	−0.115
4B 950425	−1.72	0.0	3.9e−3	−2.79±0.3	−0.739	2.5e−1	−0.053
4B 950513	−2.23	9.2e−1	9.1e−1	−0.38±0.5	−0.380	−5.8e−2	−0.191
4B 950522	−1.67	8.4e−1	8.7e−1	−1.12±1.0	−0.279	1.6e−1	−0.679
4B 950701	−2.04	1.6e−5	4.0e−3	−4.25±1.0	−0.242	4.1e−6	−0.213
4B 950701B	−2.22	1.3e−1	6.1e−1	−3.82±1.1	−0.526	−4.9e−1	0.096

TABLE 2—*Continued*

Burst Name[a]	$\beta_{\rm ave}$	χ^2 Probability:[b] Const. β	Linear β	Slope in β ($\times 10^{-2} s^{-1}$)	Correlations: Time	Intensity[c]	$E_{\rm peak}$
4B 950804	−2.48	4.6e−2	1.0e−1	13.41±6.5	0.182	5.9e−4	−0.675
4B 950818	−2.20	3.0e−3	2.7e−3	−0.90±0.9	−0.424	2.3e−2	−0.494
4B 950909	−2.41	4.6e−2	1.0e−1	0.77±0.4	0.244	−1.9e−2	0.518
4B 951011	−1.84	1.5e−1	1.3e−1	−0.91±1.0	−0.088	−3.6e−1	−0.396
4B 951016	−1.95	0.0	1.1e−2	−7.16±1.2	−0.785	−3.7e−1	0.718
4B 951102	−1.88	1.9e−2	7.9e−1	−4.89±1.1	−0.700	−8.8e−3	0.030
4B 951203	−2.27	9.8e−1	9.8e−1	−1.00±2.1	−0.276	−1.2e−1	0.352
4B 960114	−2.22	0.0	1.2e−7	−3.33±0.4	−0.617	9.5e−2	−0.277
4B 960124	−2.08	9.5e−1	9.3e−1	−0.12±2.3	−0.009	1.1e−1	−0.129
4B 960201	−2.33	8.4e−1	8.6e−1	−1.39±1.3	−0.079	−1.8e−1	−0.157
4B 960321	−2.14	0.0	6.0e−8	−2.08±0.4	−0.350	−4.5e−4	−0.206
4B 960322	−2.42	8.1e−1	9.5e−1	−1.40±0.5	−0.410	−3.3e−2	0.325
4B 960605	−2.02	0.0	0.0	−0.91±0.2	−0.142	−8.2e−4	−0.307
4B 960607	−2.06	5.3e−1	4.7e−1	−0.15±0.7	−0.097	1.1e−3	−0.346
4B 960623	−2.05	9.5e−1	9.3e−1	0.08±0.5	0.121	−9.3e−2	−0.566
4B 960807	−2.05	6.7e−1	7.2e−1	1.68±1.2	−0.029	−1.0e−1	−0.286
4B 960808	−2.11	7.6e−1	6.8e−1	−5.16±14.	−0.429	2.2e−1	0.238
4B 960831	−1.92	5.6e−4	4.4e−4	−0.08±0.1	−0.116	−1.1e−7	−0.598
4B 960924	−2.57	0.0	0.0	−3.26±1.3	−0.024	1.8e−8	−0.780
4B 961001	−2.06	2.4e−5	3.1e−2	−5.11±1.0	−0.417	−6.0e−2	0.182
4B 961009	−2.12	1.3e−3	5.5e−3	−2.02±0.8	−0.323	1.8e−2	−0.669
4B 961029	−2.50	3.8e−5	5.7e−5	0.16±0.1	−0.336	2.6e−5	−0.494
4B 961102	−2.32	1.9e−1	8.6e−1	−1.21±0.3	−0.584	4.3e−2	0.447
4B 961202	−2.38	5.1e−2	1.1e−1	−6.11±3.0	−0.473	2.2e−1	0.121
4B 970202	−1.79	0.0	0.0	−5.01±0.3	−0.493	−1.1e−3	0.140
4B 970223	−1.85	0.0	2.5e−3	−4.70±0.7	−0.509	1.3e−1	−0.411
4B 970306	−1.85	9.4e−4	5.5e−4	−0.04±0.2	0.093	−1.5e−1	−0.836
4B 970315	−1.81	0.0	0.0	−1.63±0.5	−0.420	6.3e−4	−0.597

[a]Burst names are the same as in Table 1. Bursts fitted with the COMP model are excluded from this table.

[b]Probability for χ^2, resulting from a fit to each of the two models for the behavior of β with time. Very small or zero values indicate that the model was unacceptable.

[c]Given as a signed probability. Please see the text for a full description.

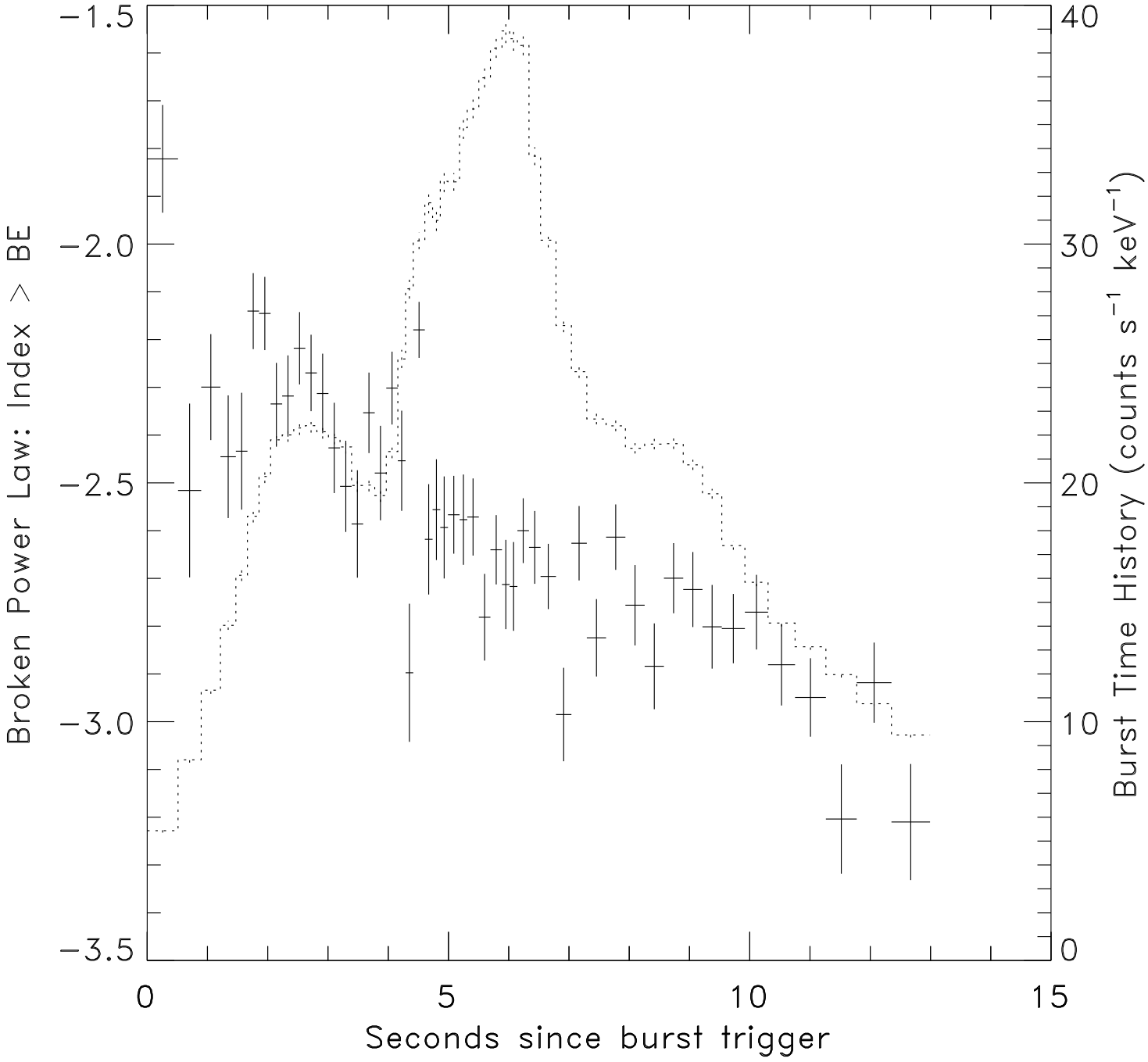
−1.5
−2.0
−2.5
−3.0
−3.5
Broken Power Law: Index > BE
40
30
20
10
0
Burst Time History (counts s^{-1} keV^{-1})
0
5
10
15
Seconds since burst trigger

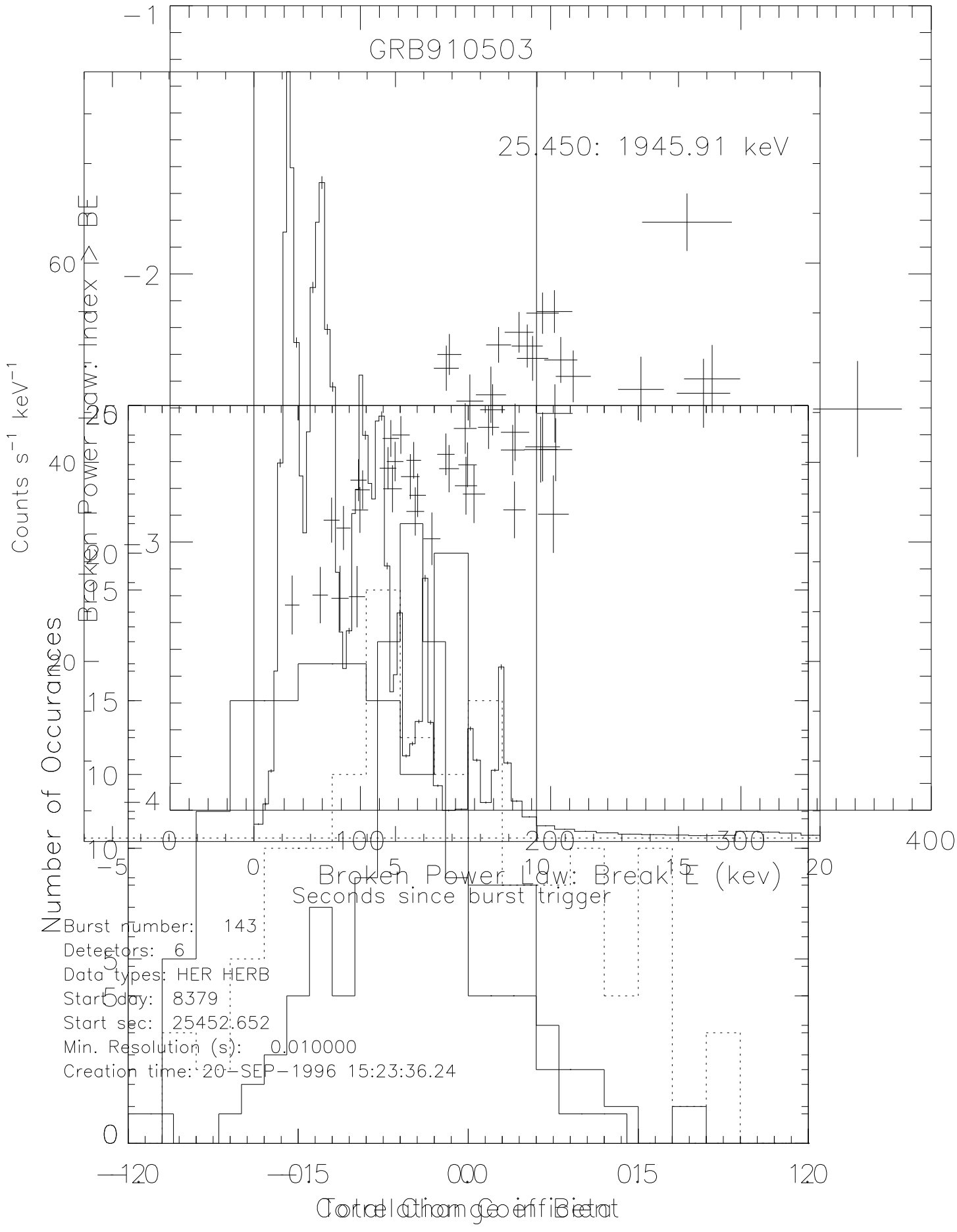
GRB910503
25.450: 1945.91 keV
Broken Power Law: Index 1 > BE
Broken Power Law: Break E (kev)
Counts s^{-1} keV^{-1}
Number of Occurances
Seconds since burst trigger
Burst number: 143
Detectors: 6
Data types: HER HERB
Start day: 8379
Start sec: 25452.652
Min. Resolution (s): 0.010000
Creation time: 20-SEP-1996 15:23:36.24

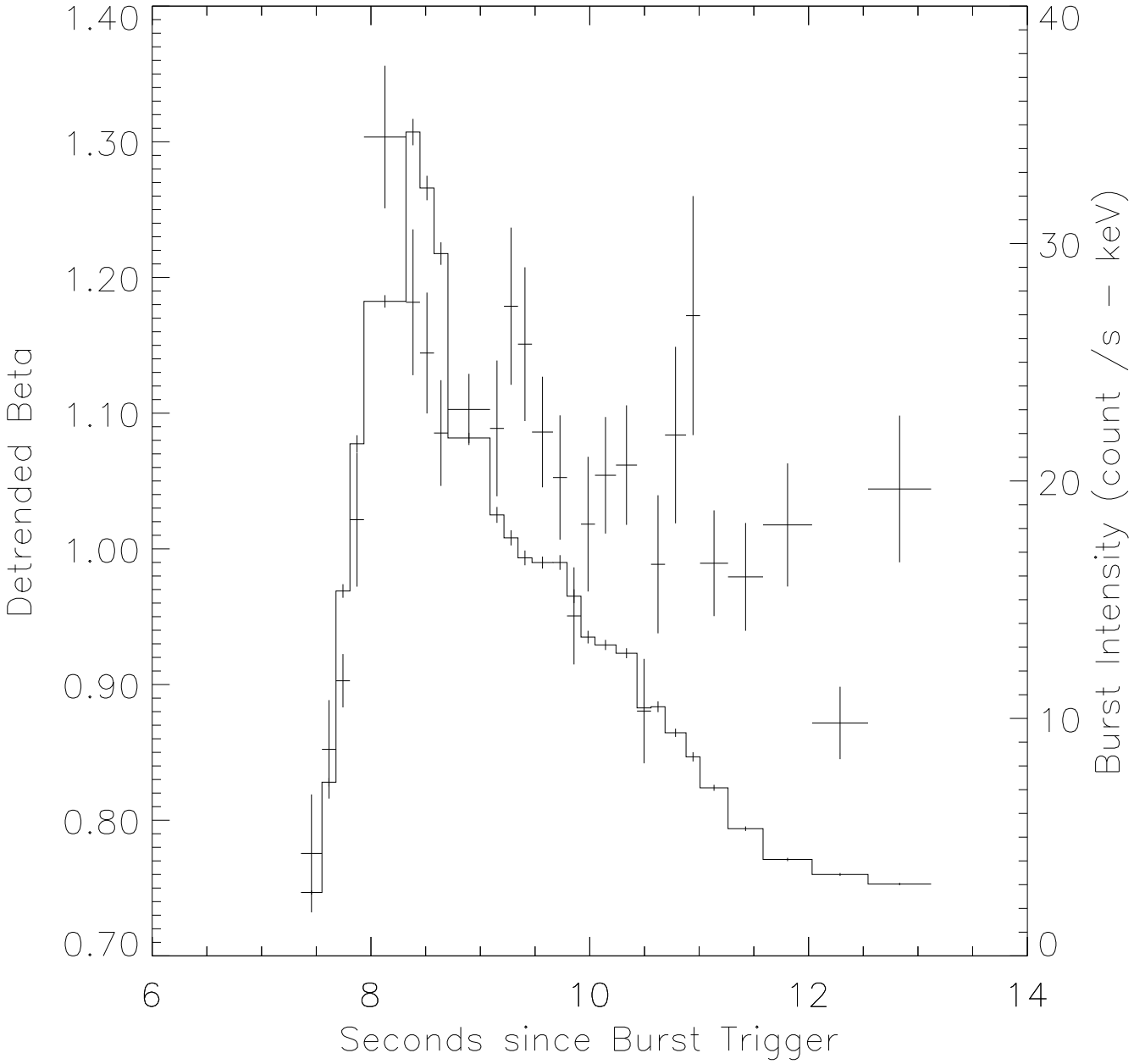
1.40
1.30
1.20
1.10
1.00
0.90
0.80
0.70
Detrended Beta
40
30
20
10
0
Burst Intensity (count /s - keV)
6
8
10
12
14
Seconds since Burst Trigger

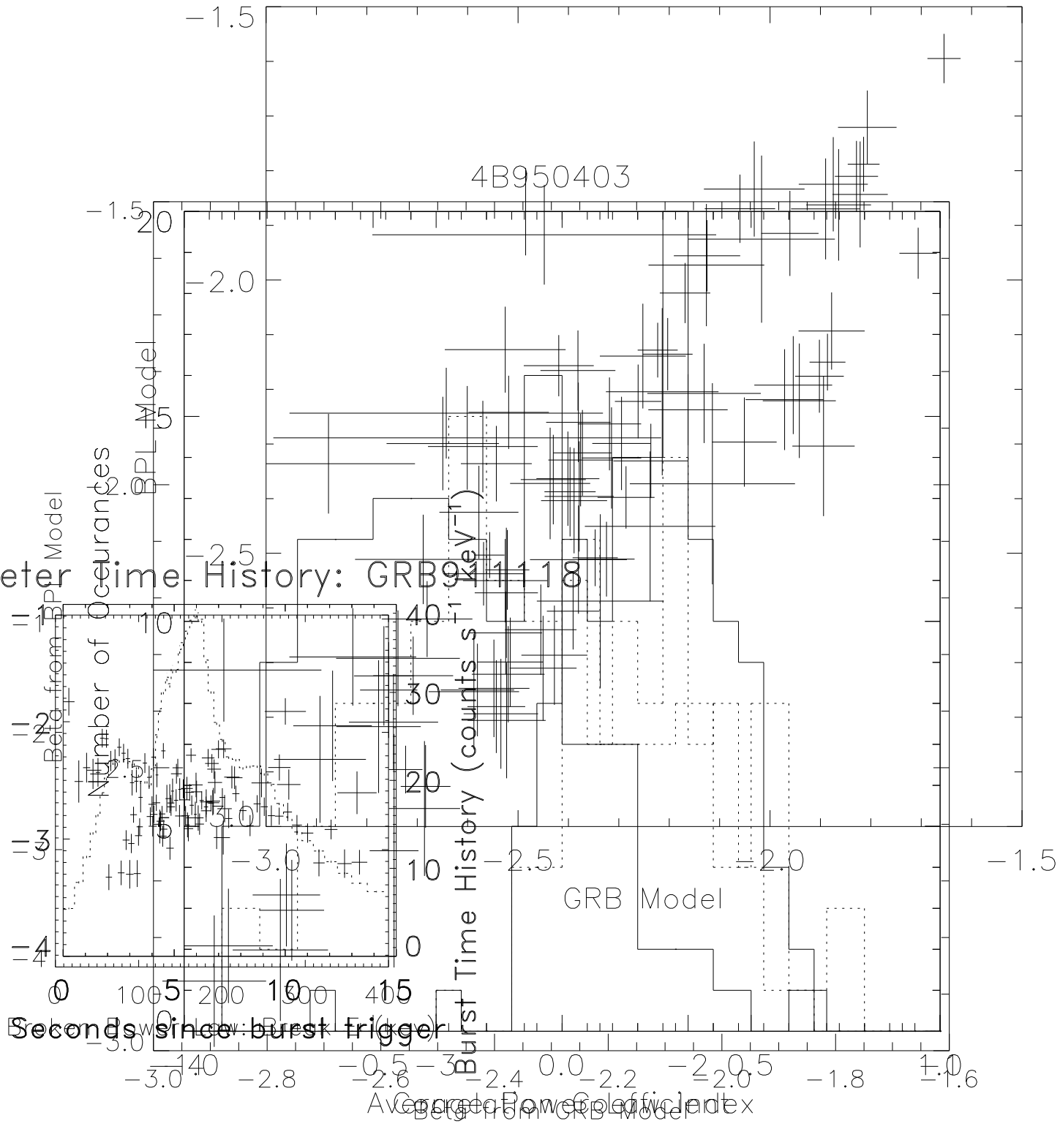
4B950403
Burst Time History (counts s⁻¹ keV⁻¹)
GRB Model
BPL Model
Beta from BPL Model
Number of Occurances
Seconds since burst trigger
Average Power Law Index
Beta from GRB Model

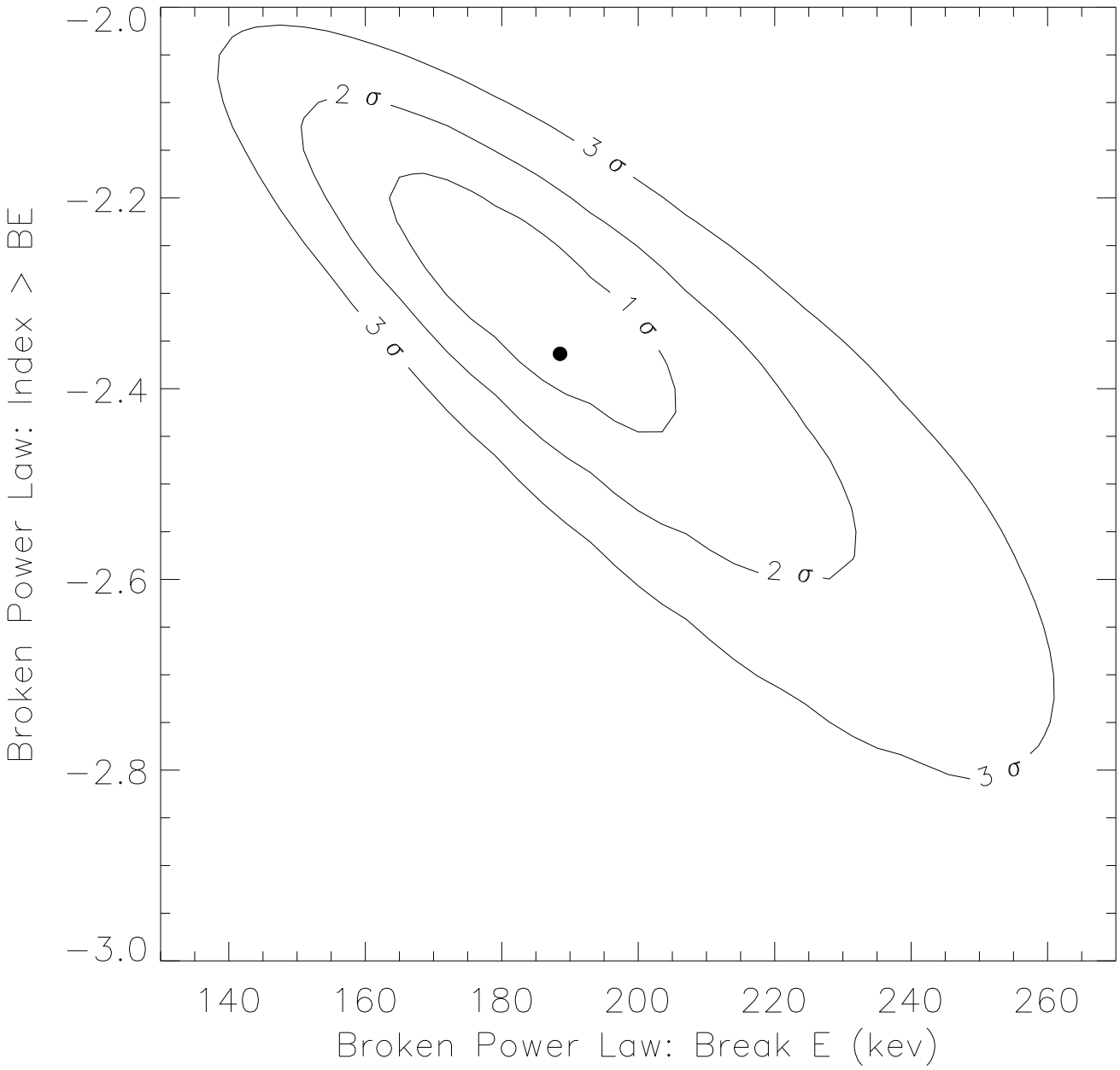
−2.0
−2.2
−2.4
−2.6
−2.8
−3.0
Broken Power Law: Index > BE
140
160
180
200
220
240
260
Broken Power Law: Break E (kev)
2 σ
3 σ
1 σ
3 σ
2 σ
3 σ

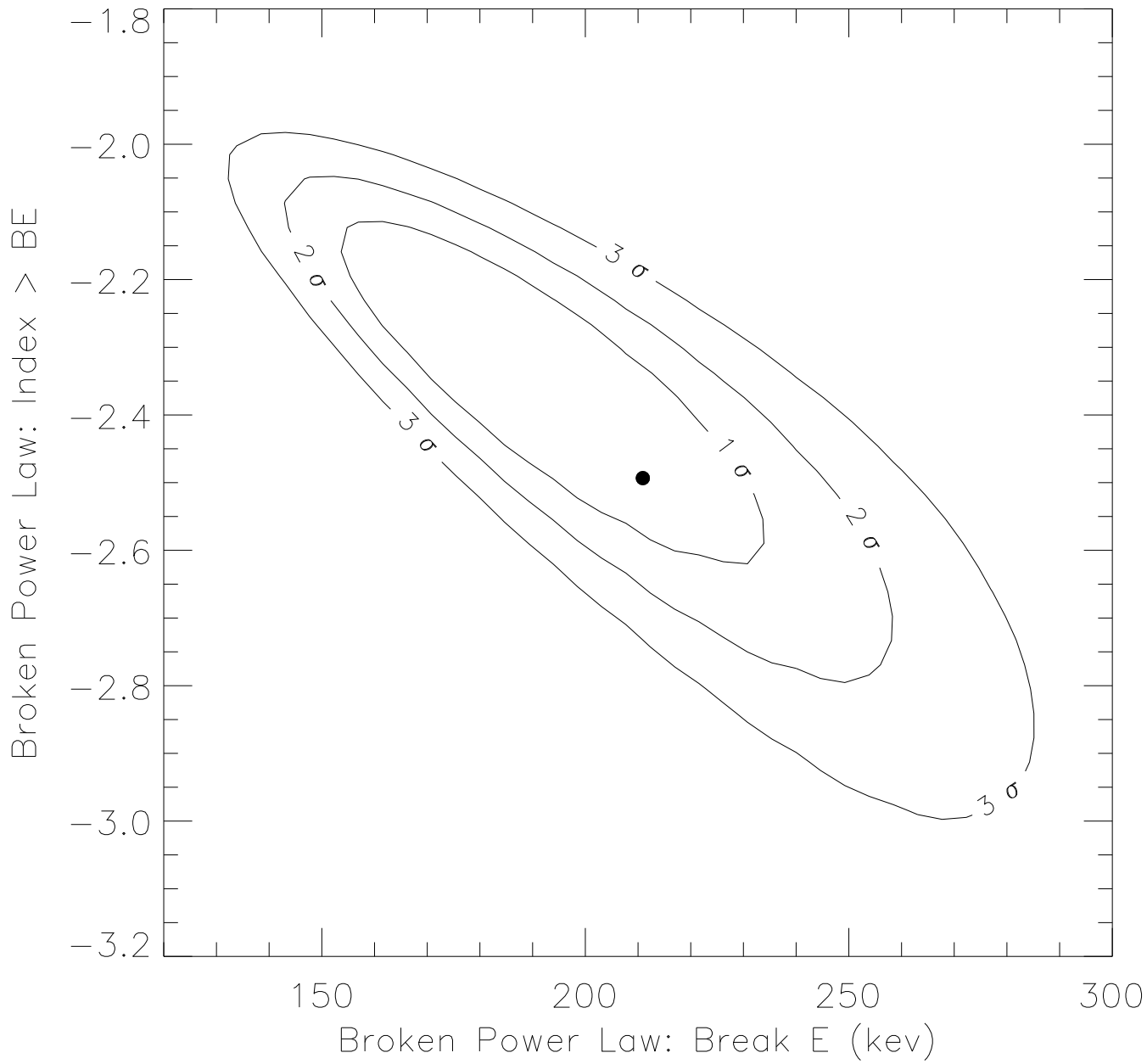
−1.8
−2.0
−2.2
−2.4
−2.6
−2.8
−3.0
−3.2
Broken Power Law: Index > BE
150
200
250
300
Broken Power Law: Break E (kev)
3 σ
2 σ
3 σ
1 σ
2 σ
3 σ

BATSE Observations of Gamma-Ray Burst Spectra. IV. Time-Resolved High-Energy Spectroscopy

Robert D. Preece, Geoffrey N. Pendleton, Michael S. Briggs, Robert S. Mallozzi, and William S. Paciesas

Dept. of Physics, University of Alabama in Huntsville, Huntsville, AL 35899

David L. Band and James L. Matteson

Center for Astrophysics and Space Sciences 0424,

University of California at San Diego, La Jolla, CA 92093-0424

and

C. A. Meegan

NASA / Marshall Space Flight Center, ES84, Huntsville, AL 35812

Received _____; accepted _____

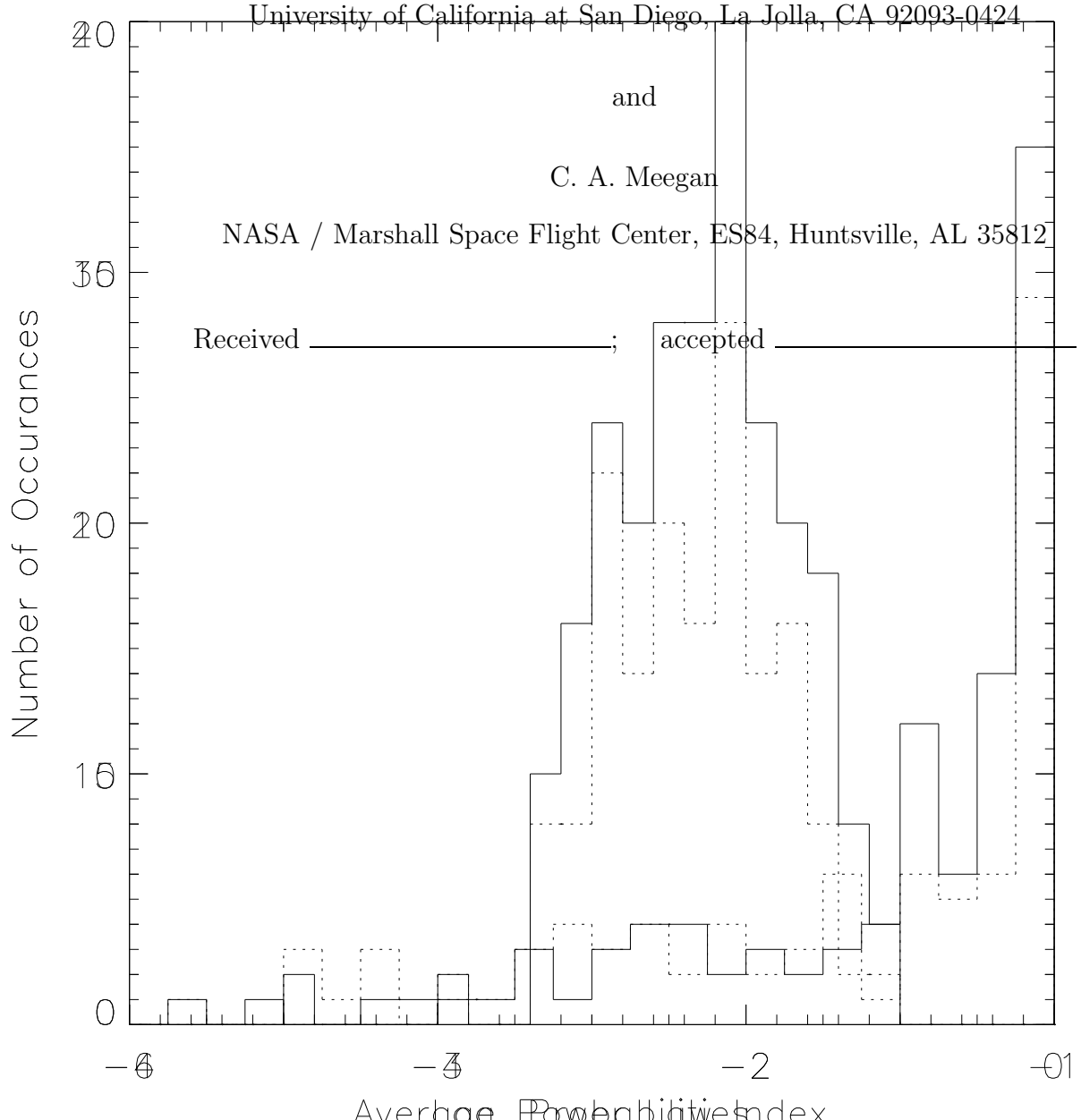

ABSTRACT

We report on the temporal behavior of the high-energy power law continuum component of gamma-ray burst spectra with data obtained by the Burst and Transient Source Experiment. We have selected 126 high fluence and high flux bursts from the beginning of the mission up until the present. Much of the data were obtained with the Large Area Detectors, which have nearly all-sky coverage, excellent sensitivity over two decades of energy and moderate energy resolution, ideal for continuum spectra studies of a large sample of bursts at high time resolution. At least 8 spectra from each burst were fitted with a spectral form that consisted of a low-energy power law, a spectral break at middle energies and a high-energy continuum. In most bursts (122), the high-energy continuum was consistent with a power law. The evolution of the fitted high-energy power-law index over the selected spectra for each burst is inconsistent with a constant for 34% of the total sample. The sample distribution of the average value for the index from each burst is fairly narrow, centered on -2.12. A linear trend in time is ruled out for only 20% of the bursts, with hard-to-soft evolution dominating the sample (100 events). The distribution for the total change in the power-law index over the duration of a burst peaks at the value -0.37, and is characterized by a median absolute deviation of 0.39, arguing that a single physical process is involved. We present analyses of the correlation of the power-law index with time, burst intensity and low-energy time evolution. In general, we confirm the general hard-to-soft spectral evolution observed in the low-energy component of the continuum, while presenting evidence that this evolution is different in nature from that of the rest of the continuum.

Subject headings: gamma-rays: bursts

1. Introduction

In the first six years of operation, the Burst and Transient Source Experiment (BATSE), on board the *Compton Gamma Ray Observatory* (CGRO), has accumulated a vast amount of spectral data on gamma-ray bursts. Although the BATSE Large Area Detectors (LADs) have only moderate energy resolution compared with the Spectroscopy Detectors (SDs), they have unprecedented effective area over their entire energy range (28 keV – 1.8 MeV). By studying spectroscopy data from the LADs for bright events such as those reported on by Ford et al. (1995), who used SD data, we can track the evolution of fitted spectral parameters with finer time resolution, and we can extend the analysis to fainter events. In this paper, we analyze 126 bursts at high time resolution, with more than 8 spectra per event, concentrating on the higher-energy behavior, where it was difficult for the SDs to obtain good statistics.

As with much of the field of GRB studies, theoretical modeling of continuum spectral emission naturally breaks into two periods: before and after the publication of the first BATSE results (Meegan et al. 1992). The paired observation of burst isotropy on the sky along with an inhomogeneous distribution of events with brightness, and presumably distance, has established the conclusion that GRBs occur much farther away, and are consequently much brighter, than previously expected. Instead of comprising a nearby Galactic disk population, burst sources either reside in a very large Galactic halo or else they are truly cosmological (we will not consider here another possible scenario: that bursts may arise in a local heliospheric halo, such as the Oort cloud [e.g.: Bickert & Greiner 1994; but also see: Clarke, Blaes, & Tremaine 1994]). Such an uncertainty in distance has had dire theoretical consequences; no single model has surfaced that can accommodate both distance scales, since such a model would have to account for luminousities that differ by ~ 10 orders of magnitude. The early theoretical work was dominated by the physics of

strong-magnetic field Galactic-disk neutron stars (see Harding 1991, for a review), which has as its basis the efficient mechanism of quantum synchrotron emission. Of course, energization of these systems was a crucial problem, in that the emission timescales are on the order of 10^{-17} s, for a typical field strength of 10^{12} G required to produce a cyclotron absorption line fundamental at ~ 20 keV, as observed in X-ray pulsars (Voges et al. 1982). Nevertheless, continuum modeling of then-current spectral data enjoyed a moderate success (many references in Ho, Epstein & Fenimore 1992).

All this began to break down with the placement of burst sources no closer than a large Galactic halo, as most of the strong-field models have restrictive luminosity constraints. Cosmological burst emission scenarios proposed to date are less predictive, but have had little time yet to mature. For the most part, interest has been focused on merging neutron stars, since the total energy budget is about right for very distant events. What happens after the merger is what distinguishes the models from each other. A simple fireball was proposed by many workers (Cavallo & Rees 1978, Goodman 1986, Piran 1994). Non-thermal emission, such as is observed in GRB spectra, is very difficult to produce in an optically-thick source, although as a fireball expands and becomes optically thin, a high-energy power-law component becomes possible. However, it was soon realized that in the environment of two colliding compact objects, baryon contamination of the fireball would pose a problem, diverting energy from the direct production of fireball radiation into the acceleration of material (see discussion in Fishman & Meegan 1995). In order to address this problem, several workers proposed that the observed gamma-ray emission originates not in the original event but is a by-product of the kinetic energy gained at the expense of the fireball. Maximal acceleration of the explosion products leads to a relativistic blast front, which can cause shocks when colliding with interstellar material, either by encountering dense knots or eventually by sweeping up matter in the path of the shock front (Rees & Mészáros 1992, Mészáros & Rees 1993). Shocks can also arise internal

to the outgoing relativistic wind, in the case where the central engine is variable (Rees & Mészáros 1994, Paczyński & Xu 1994). It is important to note that the energy distribution of the shock-accelerated particles that gives rise to the observed emission is not predicted in any of these models; however, the distributions can be inferred from observation. The most efficient radiation mechanism is synchrotron, which produces a characteristic low-energy power-law behavior (Katz 1994, Tavani 1996). The high-energy spectral shape for this model comes from the distribution of Lorentz factors for the baryons arising in the shock, which is typically a broken power law. Dispersion of blast-front velocities will give rise to observable hard-to-soft spectral evolution, both in individual pulses, as well as over the course of the entire event. Some of this behavior has been noted by Ford et al. (1995); however, the opposite behavior is also seen, as well as a mixture of both.

Apart from the details of individual theoretical models, what new can be learned from analysis of spectral data? First, we have the well-known observation that GRB spectra are non-thermal. There is good evidence that some time-averaged GRB spectra are composed of power-law emission to several 10s of MeV in energy (Matz et al. 1985, Hanlon et al. 1995). Burst emission indeed reaches very high energies, as evidenced by the single 18 GeV photon observed by *EGRET* (Hurley et al. 1994), albeit at a considerable delay from the initial outburst. This alone can say much about the distribution of particles doing the emitting, as well as the possible optical depth. Other than a multi-temperature blackbody, which can mimic a power-law spectrum over a limited energy range, non-thermal emission arises from non-thermal particles. The evolution of the particle distribution, by cooling, for example, bears a simple relationship to the evolution of the emission for many radiation mechanisms. In the fireball model, optical depths are much greater than unity during the phase in which the matter gets accelerated. Thermal emission from the fireball is not observed in the gamma-ray band (although it may be visible in X-rays below ~ 20 keV, Preece et al. 1996). In any cosmological model, it is very difficult to avoid conditions that

will rapidly lead to large optical depths via the photon-photon pair production process. This occurs in the collision of two photons where the product of their energies is greater than $2m_e^2/(1-\cos\psi)$, ψ being the angle between the photons' directions and $m_e = 511$ keV is the rest mass of the electron. Many bursts have substantial emission at 500 keV and greater, so if the high-energy emission is not to be quenched by a runaway pair-fireball, the emission must be highly beamed. The high energy power-law index and its time evolution should constrain the mechanism through which particles are giving up their energy in emission, as well as reflecting the behavior of the injection mechanism. Cases where the high-energy component comes and goes within a burst or is absent altogether may represent quenching by a mechanism that rapidly increases the optical depth, such as photon-photon pair production. In this case, it is expected that the intensity should drop during periods of quenched emission, or in other words, there should be a hardness-intensity correlation.

In this paper, we will present a study of the time-evolution of burst spectra, concentrating on the high-energy power-law component. In §2 we discuss the burst sample selection and the details of the spectral fitting analysis. The results are covered in §3 and their implications are discussed in §4. In the Appendices, we summarize the general characteristics of BATSE and then discuss in detail the energy calibration procedure for the LADs, which has made the current work possible.

2. Analysis Methodology

In order to have a sample of bursts with at least 8 spectra with count rates high enough to obtain well-determined spectral parameters, we selected a subset of bright bursts based upon either the total fluence or peak flux, as determined from the LAD 4-channel discriminator data (Meegan et al. 1996). We required a fluence (> 20 keV) greater than 4×10^{-5} erg cm^{-2}. However, the set of bursts for which the fluence can be calculated

is limited by several considerations, such as data availability, telemetry gaps in the data coverage and possible contamination of portions of some bursts with other active sources (in particular, with solar flares in the first year of the mission). Thus, we made an additional selection of those bursts which had a peak flux from 50 – 300 keV on the 256 ms timescale in the 3B Catalog (and later) above 10 photon s^{-1} cm^{-2}. Each burst was then binned in time, so that each spectrum to be analyzed had a signal to noise ratio (SNR) of at least 45 in the typically 28 to 1800 keV energy range of the HERB data (High Energy Resolution Burst data: for a description of the instrument and spectroscopy datatypes, please see Appendix A). Bursts with less than 8 spectra after binning were dropped from the sample. Most spectra in bright bursts are well in excess of this SNR, which guarantees $> 2\sigma$ of signal per energy resolution element, assuming a flat count spectrum. Roughly 20 resolution elements ($= \delta E$, the FWHM of the detector energy resolution) are required to cover the typical LAD energy range, thus the 128-channel HERB spectra are over-resolved in energy. LAD data types other than HERB are under-resolved, which is why HERB is preferred for spectroscopy. Some bursts did not have complete coverage in the HERB data (especially before a flight software revision that allowed longer accumulations during quiescent portions of a burst), in which case we used other available data, as discussed below. There are 126 BATSE bursts in our sample matching these criteria.

Background was determined independently for each channel, typically using spectra from within ± 1000 s of the burst trigger (giving at least three background HER spectra before and after the burst). The form of the background model was a fourth-order polynomial in each energy channel, where the fitted rates are time-averaged over each spectral accumulation, rather than determined at the centers. This was done to avoid underestimating the background rate at a peak or overestimating it at a valley. The SNR was determined by comparison with the chosen background model, interpolated to the time of the accumulated spectrum.

Spectra were fitted by one of several spectral forms, depending upon the best fit obtained to the average spectrum over the entire burst. The primary spectral form we used is the function of Band et al. 1992 (GRB, in table 1), which consists of two smoothly-joined power-laws:

$$\begin{aligned} f(E) &= A(E/100)^{\alpha} \exp\left(-E(2+\alpha)/E_{\rm peak}\right) \\ \text{if} \quad E &< (\alpha-\beta)E_{\rm peak}/(2+\alpha), \\ \text{and} \quad f(E) &= A\{(\alpha-\beta)E_{\rm peak}/[100(2+\alpha)]\}^{(\alpha-\beta)} \exp\left(\beta-\alpha\right)(E/100)^{\beta} \\ \text{if} \quad E &\geq (\alpha-\beta)E_{\rm peak}/(2+\alpha). \end{aligned} \tag{1}$$

The two power-law indices, α and β, are constrained such that the resulting model is always concave downwards ($\alpha > \beta$; our definition includes a possible minus sign for each index). If, in addition, the high-energy power-law index (β) is less than -2, the model peaks in $\nu\mathcal{F}_\nu$ (that is, E^2 times the photon spectrum) within the BATSE energy range. The model is parameterized by the energy of the peak in $\nu\mathcal{F}_\nu$ ($E_{\rm peak}$), rather than the energy of the break between the power laws ($E_0 = E_{\rm peak}(2+\alpha)/(\alpha-\beta)$). If the fitted value of β is very negative, roughly less than -5, the spectral form approaches that of unsaturated inverse-Compton thermal emission (Rybicki & Lightman 1979), a low-energy power-law with an exponential cut-off (COMP, in table 1). This can be viewed as a generalization of the spectral form of optically-thin thermal bremsstrahlung (neglecting any Gaunt factor), which has a low-energy power law index of -1. The GRB spectral form is a continuous function that does not allow a sharp spectral break, so that in cases where $E_{\rm peak}$ ($< E_0$) is close to the high end of the energy range for the data, β may not be well-determined. For such cases, we used instead a simple broken power law (BPL, in table 1), in order to force $E_{\rm peak} = E_0$, usually resulting in acceptable fits to the high-energy component.

Since we are concerned in this paper about the high-energy power-law behavior, we made a number of tests to be sure that our choices of spectral models do not affect the end

result. To do this, we fit several trial bursts with several different models and compared the resulting fits. The simplest test of the robustness of our fitting procedure was to fit a single power law to each spectrum above a fixed cut-off energy that was determined by the maximum over the entire set of fitted spectra in the burst of the value of the break energy E_0 between the two power-law components. This eliminated any affect the fit to the low-energy data might have on the fitted value of β. That is, curvature in the global model fit may tend to pull the local fit of the high-energy power-law index to a larger or smaller value, depending on how well the actual data tolerate the curvature. For example, the data may break more sharply than the model, which leads to a fitted value for β that is steeper than it should be. Conversely, in the broken power-law model, with no curvature built in, the high energy power law index may be pulled to a shallower value than the data require. Generally, the resulting time-history of the fitted parameters are consistent to within one-sigma errors. However, some differences were apparent when we compared the time-histories of the fitted high-energy power-law component between these two models, when both were applied to the same burst, as can be seen in figure 1. The average values of the fitted power-law indices (weighted by the errors) over the entire burst were slightly different ($\beta_{\rm ave} = -2.25$, for the GRB model fit; $= -2.16$, for the BPL), while the underlying pattern of the time-history of the parameters were similar. So while the time evolution of the high energy portion of the spectrum could be reliably traced by the fitted parameter for each model, there remains some ambiguity in the average high-energy slope. This effect should be worse for larger average values of $E_{\rm peak}$: the curvature inherent in the GRB model tends to restrict the range of energies available for determining β. The broken power-law model is plagued by a different problem: with an energy resolution (FWHM) of approximately 20% at 511 keV, we usually cannot determine the exact position of the break energy using LAD count spectral data.

With the fitted values of the break energy and β possibly closely correlated, the

reported 1σ error on each parameter is only part of the story. That is, the errors are most accurately determined from a multi-dimensional χ^2 contour plot for the correlated parameters, as seen in figure 2. The contours represent $\Delta\chi^2$ values appropriate for one parameter of interest, so that the 1σ contour is at $\Delta\chi^2 = 1$ (for this figure only; usually, one would be interested in both parameters jointly, resulting in larger contours). The 1D 1σ error limits are formed by the maximum and minimum of the error ellipse projected onto the axis of the parameter being considered. The actual 1σ errors reported here are obtained from the diagonal elements of the covariance matrix for each fit; this is equivalent to $\Delta\chi^2 = 1$, with the additional assumption that the fitted parameter value lies in the center of the error interval. By taking into account the joint error between the parameters, $\Delta\chi^2$ is increased to 2.3, so that the fitted values of the high-energy power law index can be reconciled to within one or two sigma between the two different spectral forms.

The fact that we obtain acceptable fits with different spectral models reflects on the ambiguity of the forward-folding process. Given the detector response, a count recorded in a given data bin could have come from a photon of any number of different energies, all greater than or approximately equal to the nominal energy range of the data bin. The dominant component of the response at low energies is the resolution-broadened photo-peak, centered on the photon energy. On top of this are counts derived from incomplete absorption of higher-energy photons in the detector, the off-diagonal component of the response. Consistent with the constraints imposed by the detector model, including especially the energy resolution, a given photon model folded through the detector response matrix will redistribute the predicted counts to best agree with the observed data. Thus, the solution to the forward-folding spectral fitting problem is not unique.

Table 1 summarizes global aspects of the fits performed for each burst. We use the 3B catalog name (Meegan et al. 1996) and BATSE trigger number to identify each burst,

followed by the number of the detector with the smallest zenith angle with respect to the source, the spectral model used for fitting, the number of fitted spectra, the time interval selected for fitting, the average of the fitted values for $E_{\rm peak}$ and the fluence, summed over the fitted spectra. In cases where there are two or more detectors reported in the third column, a summed 16 energy channel data type (MER) was used, usually for lengthy events which ran out of HERB memory before the end of the burst. For a small number of cases where other data types were absent, we use SD 256 energy channel data (SHERB); these are indicated in column three with an 'S' appended before the detector number. The three models used in our analyses are indicated by their respective mnemonics (introduced above) in column four. The COMP spectral form has one less parameter than the others: there is no fitted high-energy power-law index. However, each of the models shares three corresponding parameters: amplitude, low-energy power-law index and $E_{\rm peak}$ (or spectral break energy for the broken power-law model). In the last two columns we indicate the average value for $E_{\rm peak}$ in keV and the total fluence for the fitted interval in erg cm^{-2}. Notice that three of the four bursts that required the COMP model did so because the high energy power law was completely unconstrained; indeed, for these bursts $E_{\rm peak}$ was also unconstrained, as the average value is far greater than the energy of the highest channel available in the data (typically 1800 keV). In the following analyses, we shall exclude these four bursts, since no trend in the high-energy power law index can be determined with our data.

3. Observations

We should like to know several things concerning the behavior of the high-energy power-law as a function of time. First of all, is it constant? If not, does the index change smoothly with time, as with the hard-to-soft spectral evolution observed in the $E_{\rm peak}$

parameter by Ford et al. (1995)? If the behavior is not smooth, is it correlated with other observable features in the burst time history, such as the instantaneous flux or the evolution of the low-energy spectral parameters? To investigate these questions, we subjected the fitted values of the high-energy power-law index to several statistical tests, and evaluated the probability the outcome of each could have occurred randomly. The results of our analyses, shown in table 2, are described below. Each row of the table is indexed in the first column by the trigger name from table 1. For each burst, this is followed by the weighted average of β, the probability that a constant β describes the data, the probability that a linear trend in β describes the data, the slope from a linear fit to the time series of β, and the probabilities that the fitted values of β are correlated with time, the burst time history or with the time series of $E_{\rm peak}$.

To start with, we would like to test the hypothesis that β is a constant over the entire burst. In order to do this, we first computed a weighted average of the fitted values of the high-energy power-law index (which we will denote as β, regardless of which model we used for the fit) over the time interval selected for each burst. The weight applied to each term in the average is the square of the 1-sigma error, σ_i, of the fit:

$$\beta_{\rm ave} = \sum_i \Big(\frac{\beta_i}{{\sigma_i}^2}\Big) \Big/ \sum_i \Big(\frac{1}{{\sigma_i}^2}\Big). \qquad (2)$$

In cases where the fit resulted in an undetermined value for β for an individual spectrum, the value was thrown out of the weighted average. It should be noted that, with weighting of the individual values, as well as the elimination of undetermined values, the result is different from the value of β obtained from a fit to the integrated spectrum. The third column in table 2 gives the probability for χ^2 obtained by subtracting the weighted average from the actual fitted values in each burst. The χ^2-values are calculated assuming the model, and thus a small value (such as $< 10^{-4}$) indicates a problem with the assumption and thus the likelihood that the model is false. A histogram of the logarithm of these

probabilities in figure 3 (*dotted line*), shows that for some bursts, at least, a constant β is consistent. What is not shown are the 30 bursts for which the probability is essentially zero. Including the bursts for which the log. of the probability is less than -4, we have 42 out of 122, or 34% of the total sample, that are not consistent with a simple, constant model in β. It is extremely unlikely that this distribution occurs randomly.

The distribution of $\beta_{\rm ave}$, shown as a histogram in figure 4, improves on earlier work by Band et al. 1993, with a larger sample and better statistics per burst. However, the resulting values from these two studies cannot be compared directly, since here we have weighted each fitted value of β by the parameter error, while in the previous study the fits were made to average spectra, which are implicitly weighted by intensity. Finally, the sample sets are different: the selection of events in Band et al. 1993 was based upon peak counts, not fluence or peak flux, since these were unknown at the time. The median value for the sample is -2.12, with an absolute deviation width of $w_{\rm ADev} \equiv \frac{1}{N}\sum_{j=1}^{N} \mid x_j - x \mid = 0.23$ (where x_{med} represents the median, which minimizes the absolute deviation), compared with the standard deviation of 0.30. The distribution has an extended negative tail that gives it a skew value of -0.73 (the skew is defined as the dimensionless third moment of the distribution, and is 0 for a Gaussian), large compared with the expected standard deviation of the skew of $\sqrt{15/N} = 0.35$ for a purely Gaussian distribution. Given the large variation of other spectral parameters, such as $E_{\rm peak}$ which has a distribution at least as wide as the range of possible values, it is surprising that the high-energy behavior is so restricted. Plotted over the total distribution in figure 4 is a histogram of those bursts for which β is consistent with being constant (log. probability > -4 from figure 3).

Obviously, a constant value of β is not acceptable for many bursts. A clear example of this is presented in figure 5, which shows the time history of β during 3B911118 and is an example of general hard-to-soft spectral evolution in β. The Spearman rank-order

correlation of β with time is given in column 6 of table 2. The correlation coefficient r is distributed between -1 and 1, and can be converted through the combination

$$t = r\sqrt{\frac{N-2}{1-r^2}} \tag{3}$$

to a Student's t-distribution for $N-2$ degrees of freedom. Unlike the χ^2 probabilities, correlation coefficients that are not consistent with roughly a normal distribution around 0 reject the null hypothesis that no correlation exists; therefore, small probabilities indicate significant correlation. The probabilities associated with r, calculated using equation 3 along with the number of spectra fitted (N) from column 5 of table 1, reveal that a trend in the data exists for at least 21 of the events at the 10^{-3} significance level or smaller. This is a robust estimator for correlation; it indicates when a correlation is almost certainly present. However, the Spearman test does not take into account the errors for each point, so if there are a large number of outliers with large errors in the sample, the test will come up with poor results. Figure 6 presents the distribution of the time correlation coefficients (*solid line*). The bulk of the distribution consists of negative correlations, indicating an anti-correlation of the power-law index with time, or hard-to-soft spectral evolution.

A linear fit to the time history of β also indicates whether there is a monotonic trend in the data, while accurately treating the errors in the fitted power-law indices. The fifth column of table 2 gives the linear coefficient, or slope, of such a fit, having the units of change in β per unit time, or s^{-1}. The sign is such that hard-to-soft spectral evolution (β grows more negative in time) results in a negative slope. The χ^2 probability for this fit is given in the fourth column of the table and the distribution is also plotted on figure 3 (*solid line*). In 24 cases out of the total sample, the log. probability was less than -4, indicating that the linear trend was a poor model of the data for those events. Comparing this result to that for the model of constant β, however, more bursts had acceptable fits to a linear trend at the same significance level (98 compared with 80 out of 122). There are far

more cases of hard-to-soft spectral evolution (100) than there are for soft-to-hard evolution, which was already evident in figure 6. The first spectrum in many bursts is the hardest (see figure 5), while at the same time being one of the weakest. Since each burst has a different duration, the slopes in physical units may not be directly comparable. However, the fitted slope in β times the duration of the fitted time interval, from column 6 of table 1, is a dimensionless parameter ($\Delta\beta$) that represents the total change in β, assuming that the evolution in β is linear (as it is for the majority of the sample). Figure 7 shows that the distribution of $\Delta\beta$ has a single, roughly symmetric peak centered on -0.374, with one outlier (not shown in the figure). The median absolute deviation width of the distribution is $w_{\rm ADev} = 0.392$, compared with a standard deviation of $\sigma = 0.516$. This argues that a single physical process characterizes the majority of the sample; and again points out that hard-to-soft spectral evolution is typical behavior for the high-energy power-law component. Physical mechanisms for burst energetics should account for this, possibly via depletion of a reservoir of energy that is available for the burst. Otherwise, it may be that when the high-energy portion of the emission changes beyond this point, the total emission is quenched.

The linear fit to the power-law indices does not characterize the distribution well for many bursts (24 out of 122), indicating that other types of behavior may be present. Figure 5 serves as an example of a burst that has strong hard-to-soft spectral evolution but where the linear fit is unacceptably poor. The residuals to the fit have considerable scatter that is correlated in successive time bins in several places on the figure. It is these residual patterns that we are interested in. Two possibilities are easily tested: there may be a correlation between the high-energy behavior and intensity within a burst (clearly not the case for 3B 911118 in figure 5), or the high-energy spectrum may be correlated with the evolution of the low-energy spectrum. Burst 3B 911118 is an example of this behavior, as can be seen in figure 8, where the fitted values of $E_{\rm peak}$ (representing the low-energy

behavior) and β have been plotted against each other.

For the case of correlation between hardness (as measured by the high-energy power-law index) and intensity (measured as total count rate in the fitted energy interval: ~ 28 – 1800 keV), we applied two statistical tests to the data and multiplied their probabilities in order to screen for candidates. The tests (described below) are likely to be correlated; however, each measures the hardness-intensity correlation differently, so that their product combines the best of each. We set the threshold for significance at 10^{-6} for the product, so to avoid false positives as much as possible. In both tests, we removed the first-order trend in the data by dividing by the linear fit to the power-law indices (which is described above). We do this, despite the fact that many bursts don't show a linear trend in the high-energy power-law index, since there are a considerable number of bursts that do have a significant correlation between β and time, while the burst intensity manifestly does not: a typical burst will have overlapping regions of both positive (rising portions) and negative (falling) correlation with time, so that the whole ensemble of β values has no correlation. The overall linear trend may be larger than the amplitude of the residuals of the fitted linear model (this is the case in figure 5), in which case there is no significant hardness – intensity correlation as determined by β alone. After detrending, the residuals may or may not be correlated with intensity. The Spearman rank-order test is relatively unequivocal: that is, if the resulting probability is low enough, then the desired correlation definitely exists. However, the converse is not true: the test can fail badly since it ignores the one-sigma errors in the fitted power-law indices. For this reason, we also have calculated the linear correlation coefficient between the detrended values of β and intensity, where the inverses of the variances on the detrended power-law indices are used to weight their contribution (Press et al. 1992). For this case, individual, poorly-determined indices that are only a few sigma away from being consistent with correlation contribute the same as well-determined ones closer to the center of the distribution. In practice, while this kind of

test is a poor indicator of whether an observed correlation is statistically significant, it is a rough indication of the strength of a correlation under the assumption that a correlation definitely exists, so the two statistical tests we've chosen complement each other, to a certain extent. Their product selects those bursts that have low probabilities (indicating strong correlation) from both tests (assuming that by detrending no significant correlation was introduced that was not present in the original data). We have indicated the combined probabilities from both tests in the seventh column of table 2 and also indicate the sign of the linear correlation coefficient. Since the power-law indices were detrended, a positive sign indicates a negative actual correlation; that is, the high-energy behavior is opposite that of the burst time history. An example of positive correlation in the detrended values of β for 4B 960924 is shown in figure 9. A small number of bursts (9), have significances less than 10^{-6}. Of these, 6 are examples of positive correlation. A larger number (24) are significant at the 10^{-4} level.

Another possible type of behavior in β that is testable with our data is a correlation with the low-energy spectral evolution. The most obvious such behavior is the hard-to-soft spectral evolution of $E_{\rm peak}$, discussed by Ford et al. (1995). $E_{\rm peak}$ is a good measure for overall spectral evolution since it marks the peak in the power output of the spectrum per log. decade. Of course, $E_{\rm peak}$ is not defined for those portions of a burst where $\beta > -2$; in that case, we substitute the break energy of the spectrum instead. In addition, we wish to check for higher moments of correlation than is possible with a linear trend of β in time, which was discussed above, such as the evolution of β within individual peaks of a burst. In table 2, column 8, we calculate the Spearman rank-order probability that the distribution of β for a given burst is correlated with the distribution of $E_{\rm peak}$, which stands in here for the low-energy behavior. The best example of correlation with $E_{\rm peak}$ is shown in figure 8, which is a plot of the two fitted parameters against one another for 3B 911118. Out of 122 bursts, 15 bursts have probabilities less than 10^{-3}, indicating correlation, and out of these

only 5 have significant hard-to-soft spectral evolution, as measured by how many sigma the slope in β in table 2, column 5, deviates from 0. The important point is that, whereas hard-to-soft behavior can be demonstrated for large numbers of bursts in the evolution both $E_{\rm peak}$ and β, this behavior is generally not correlated between the two. Indeed, hard-to-soft evolution of $E_{\rm peak}$ within individual peaks of a burst is not typically observed with β, otherwise, far more instances of correlation between the two would have been observed.

4. Discussion

In this series of BATSE spectral analysis papers, we have demonstrated several times the universal suitability of the 'GRB' spectral form for fitting burst spectra, whether it is applied to the total spectrum averaged over the burst (Band et al. 1993), to time-resolved spectroscopy of bright bursts in the SD data in Ford et al. (1995), to joint fits of time-averaged spectra of bright bursts with the low-energy discriminator data (Preece et al. 1996; although we see the model break down with low-energy excesses observed in 15% of GRBs) and now to time-resolved spectroscopy of bursts observed mostly with the BATSE LADs. In figure 4, we now see that there is evidence of an average high-energy power law index that is ~ -2 in a large number of GRBs. In addition, the variance of this index over the sample is similar to that obtained by Pendleton (1994a), using BATSE LAD discriminator data.

Table 2 presents evidence that β is not constant for 42 out of 122 bursts in our sample. The typical change in β over an entire burst, ~ 0.4 (figure 7), is small compared with the average value of $\beta \approx -2.1$. We should consider which of the many emission models proposed for GRBs are consistent with these observations. A -2 power law slope is evidence for single-particle cooling, from either synchrotron losses or Compton scattering (Blumenthal & Gould 1970). Typically, one would integrate the energy loss rate over the

particle distribution; however, particles that are relatively cool with respect to their large, possibly relativistic bulk motion can be treated as monoenergetic in interactions with static external particles or fields. Bremsstrahlung losses are another matter. Such scenarios have been proposed for bursts of cosmological origin for external shocks, (Rees & Mészáros 1992 & Mészáros & Rees 1993) as well as for synchrotron shocks (Katz 1994 & Tavani 1996). It should be noted that the cooling timescale for most expected processes, especially those like synchrotron that involve magnetic fields, is far shorter than observed burst lifetimes by many orders of magnitude. In fact, this is a common problem with GRB models: an unspecified energy storage mechanisms usually must be invoked in order to extend the emission. Relativistic bulk motion, which is necessary to ensure that bursts do not degenerate into a pair fireball, can multiply the lab-frame lifetime by the Lorentz factor, usually considered to be on the order of 1000. This is not nearly long enough for processes such as synchrotron emission whose characteristic timescale may be on the order of 10^{-17} s. Clearly, in bursts, there is a reservoir of energy, possibly the protons that carry the bulk of the kinetic energy in the blast wave.

It appears that hard-to-soft spectral evolution predominates over soft-to-hard, as observed already in Norris et al. (1986), Ford et al. (1995) and Band (1997). In our study, the high-energy behavior follows this trend at the greater than the 3σ level in 50 out of 122 cases, while the opposite is true for only 5 bursts at the same significance. This is independent of the low-energy behavior; indeed, we have a significant correlation with the low-energy behavior in only 15 cases and out of these, 5 have significant hard-to-soft spectral evolution. Taken together, we have evidence that the high-energy behavior is very much independent of the rest of the spectral evolution of a burst; in 35% of the cases, there is hard-to-soft spectral evolution, and no evolution in most of the rest, only 10% of all bursts failing the linear fit χ^2 test.

As seen in figure 4, there is a small group of 'super-soft' bursts characterized by $\beta_{\rm ave} <\sim -3.0$. Along with 4B 970111, which was an extremely bright burst with no apparent high-energy power law component (it was fitted with the COMP model), we have three such events. Several of these have no detectable emission above $\sim$ 600 keV. This behavior is similar to the 'no high-energy' bursts of Pendleton et al. (1997), which were shown to be homogeneous in space. Since most of the homogeneous bursts were relatively weak, compared with the entire sample, here we must be observing the brightest few of that set, rather than 20%, as reported in Pendleton et al. (1997). There may actually be a continuum of burst properties, with these bursts representing the furthest extreme. Bursts in this extreme (as well as some portions of other bursts that have very steep high-energy power laws) may be an indicator that some emission-limiting phenomenon such as pair-plasma attenuation may be at work. Indeed, in many cases, spectra in these bursts can be fitted by a spectral form that does not require a high-energy power-law (such as the COMP model). This also fits in with the observation that such events are typically weaker than average. In the context of shock models of GRBs, several parameters of the particle energy distribution determine the resulting spectrum. These may be factors such as the shape of the distribution, whether it is a power law, the maximum energy or the bulk Lorentz factor. It is very likely that the maximum energy of the accelerated particle distribution resulting from the shock could be drawn from an enormous range (out to several GeV, at least), depending on the conditions at the shock. Thus, the super-soft bursts may be representative of particle distributions that arise from weak shocks, affecting the shape or maximum energy in such a way to limit the high-energy emission.

5. Summary

In this study, we have looked in detail at the temporal behavior of the high-energy power-law portion of GRB spectra from a sample of 126 bursts selected by either high flux or fluence. The average over all fitted spectra of all bursts in the sample for the high energy power law index (β) is ~ -2.12, although fitting a constant, average index to the time history of β in each burst resulted in unacceptable χ^2 values for 34% of the bursts. In addition, of those bursts in which β is not constant, a large number (100) show hard-to-soft spectral evolution, compared with those that have an overall, significant soft-to-hard trend. The total change of β over the time interval chosen for fitting has a single-peaked distribution, centered on -0.37, indicating that theoretical modeling will have to explain why most bursts favor this value. In several bursts, the hard-to-soft spectral evolution is correlated with similar behavior at lower energies. We also find that some bursts have a significant correlation between β and the burst time history, or equivalently, instantaneous flux. Some bursts in the sample were too soft to be characterized by a high-energy tail, while there are intervals in many bursts that have similar behavior, as has been reported by Pendleton et al. (1997). Taken together, these results show that the high-energy spectral component has a rich life, independent to a large extent of the behavior of much the rest of the spectra.

Many thanks to Surasak Phengchamnan and Peter Woods for generating a list of post-3B catalog fluences and peak fluxes. We also thank the anonymous referee, for comments that lead to improvements in the paper. This work could not have been possible without our spectral analysis software (WINGSPAN). It is publicly available from the BATSE webserver: http://www.batse.msfc.nasa.gov/. BATSE work at UCSD is supported under NASA contract NAS 8-36081.

A. BATSE Large Area Detectors

The BATSE LADs are a set of eight identical NaI detectors, which are mounted on the corners of the *CGRO* and oriented to ensure maximum all-sky exposure. Perhaps the most important feature of the BATSE instrument is its ability to localize a transient cosmic source by the comparison of counting rates in the four detectors that directly see it (Pendleton, Briggs & Meegan 1996). This is an invaluable aid to spectroscopy, since the detector response is a strong function of the source-to-detector axis angle, with differing responses at different energies (Pendleton et al. 1995). Thus, without location information, the detector response cannot be fully modeled, and spectral model fitting cannot be done accurately.

Spectral data from the LADs are compressed to either 128-channel high energy resolution background and burst data (HER and HERB datatypes, respectively) or 16-channel continuous background or medium energy resolution burst data (CONT and MER datatypes). The HER background data are typically accumulated over 300 s, while the CONT data are always accumulated every 2.048 s. The HERB burst trigger data are accumulated in a time-to-spill mode: one spectrum is generated in the time it takes to record 64 k counts (in units of 64 ms), currently with a fraction of the last available background rate subtracted, to ensure that longer accumulations are taken over periods when the burst has returned to background levels. This fraction was zero for roughly the first half of the mission, so bright, highly-variable bursts commonly ran out of available memory. For the four detectors recording the highest count rates at the time of the trigger, there are 128 spectral accumulations, each 128 ms in duration or greater. The lowest seven channels of the 128 are at or below the analog lower-level discriminator (LLD), and are unusable; the highest few channels suffer from saturation in the pulse amplifier and thus are also thrown out. The remaining channels are spaced quasi-logarithmically in energy, falling

between approximately 28 keV and 2 MeV, with the exact energy coverage of each channel in each detector determined by a channel-to-energy conversion algorithm. It is important to note that these energy ranges are quite stable through the mission, due to automatic gain control of the PMT voltages. The energy resolution of the LADs was measured on the ground to be $\sim 20\%$ at 511 keV (Horack 1991), and has been quite stable in orbit.

B. Energy Calibration Methodology

In order for spectroscopy to be possible with the LAD HERB data, we have had to apply a correction to the channel-to-energy conversion algorithm that was developed before the launch of the spacecraft. Measurements of several calibration sources at known energies resulted in an empirical relationship between channel number and channel energy threshold (Lestrade 1991). The function fitted was essentially linear, with a small non-linear term (significant only at low energies), proportional to the square root of the channel number; thus there are three fitted parameters. After several bright bursts were observed in orbit, it became clear that each detector had a systematic pattern of residuals, localized to the low end of the count spectrum. With the assumption (tested below) that these features are intrinsic to each detector, and not a function of detector-to-source angle or source intensity, we developed a method of calibration using in-orbit data.

In order to properly calibrate the detectors, we must choose bright objects with well-known spectral properties, seen by each detector. Solar flares are generally not usable, since they are rarely seen by half the detectors, due to the pointing constraints of the spacecrafts solar panels, and their spectra are typically too soft. Earth occultation data from the Crab nebula was used by Pendleton (1994b) to calibrate the 16 channel CONT spectra. However, this was not feasible for HER spectra because of telemetry constraints. We are left with bursts themselves. Averaged over their entire time history, at least some

bursts can be expected to have a fairly smooth spectrum (Band et al. 1993). Spectral features, such as lines, will tend to average out over time and in the LAD data will not contribute much overall, due to the moderate energy resolution of the detectors. For bright bursts, we can precisely determine the average spectrum from the well-calibrated SD spectral data (Band et al. 1992) to use as a constraint in a joint fit with the LAD spectral data. The single time-averaged spectrum from the calibration burst is no longer available for spectroscopy; however, individual spectra from the burst are still usable for our analyses, for two reasons. First, continuum spectral fits are robust, in that they sample broad features in the spectrum, rather than the behavior of individual channels. Second, the calibration affects only the lowest channels of the spectra, and therefore does not affect spectral fitting of the high-energy power-law index, as long as it is determined by counts above $\sim$ 150 keV. In the present paper, we needed to obtain a global fit to each spectrum, so it was important to calibrate the lower channels as well as possible.

The general process is iterative: we jointly fit the LAD and SD spectral data for an entire outburst interval in a bright burst, using the standard calculation for the LAD data energy thresholds. The residuals of the fit to the LAD data are used to determine by how much to adjust the energy of each data channel edge in order to bring the count rate closer to the model rate. With this new set of edges, a new detector response matrix (DRM) is generated to account for the shift in the position of the photopeak with the change in output edges and the accompanying change in total response. The photon model is recalculated with the new DRM and count rate residuals are again determined. Since the pre-flight calibration produces acceptable agreement above $\sim$ 150 keV, we limited the re-calibration to energies below 150 keV. We also enforced a fixed lower energy for HERB data channel 7 ($\sim$ 25 keV), to limit the corrections to apply only to channels above the energy of the LLD, as this is currently not modeled in the DRM. The freedom of lower-energy edges to wander is highly constrained in the joint fit with the SD data, which overlap the LAD

energy range and can extend the continuum fit to lower energies by up to 10 keV. Each of the edges within the two limits are recalculated in each new cycle until the value of χ^2 for the fit stops decreasing. For each of the eight detectors, one calibration burst yields a set of offsets of new edges relative to the original edges, which can then be applied to all bursts observed by that detector throughout the mission. We have extensively tested the hypothesis that the non-linearities are intrinsic to the detector by examining the residuals to spectral fits of several very bright bursts in each detector with the new calibration. We have found excellent agreement of the calibration results between bursts, regardless of the angle, intensity or hardness of any given event.

REFERENCES

Band, D. L., 1997, ApJ, 486, in press

Band, D. L., et al. 1992, Exp. Astron., 2, 307

Band, D. L., et al. 1993, ApJ, 413, 281

Bickert, K. F., & Greiner, J. 1994, Compton Gamma-Ray Observatory Symposium, M. Friedlander, N. Gehrels & D. J. Macomb, New York: AIP, 1059

Blumenthal, G. B., & Gould, R. J. 1970, Rev. Mod. Phys., 42(2), 237

Cavallo, G., & Rees, M. J. 1978, MNRAS, 183, 359

Clarke, T. E., Blaes, O., & Tremaine, S. 1994, AJ, 107, 1873

Fishman, G. J., & Meegan, C. A. 1995, ARA&A, 33, 415

Ford, L. A., et al. 1995, ApJ, 439, 307

Goodman, J. 1986, ApJ, 308, L47

Hanlon, L. O., Bennet, K., Williams, O. R., Winkler, C, & Preece, R. D. 1995, Ap&SS, 231(1), 157

Harding, A. K. 1991, Phys. Rep., 206, 327

Ho, C., Epstein, R. I., Fenimore, E. E. 1992, Gamma-Ray Bursts, Cambridge: Cambridge

Horack, J. M. 1991, Development of the Burst and Transient Source Experiment (BATSE), NASA Reference Publication 1268

Hurley, K., et al. 1994, Nature, 372, 652

Katz, J. I. 1994, ApJ, 432, L107

Lestrade J. P. 1991, NASA internal memo

Matz, S. M., et al. 1985, ApJ, 288, L37

Meegan, C. A., et al. 1992, Nature, 355, 143

Meegan, C. A., et al. 1996, ApJS, 106, 65 (BATSE 3B Catalog)

Mészáros, P. & Rees, M. J. 1993, ApJ, 405, 278

Norris, J. P., et al. 1986, ApJ, 301, 213

Paczyński, B, & Xu, G. 1994, ApJ, 427, 708

Pendleton, G. N., et al. 1994, ApJ, 431, 416

Pendleton, G. N., et al. 1994, The Second Compton Symposium, C.E. Fichtel, N. Gehrels & J. P. Norris, New York: AIP, 749

Pendleton, G. N., et al. 1995, NIMSA, 364, 567

Pendleton, G. N., et al. 1997, ApJ, submitted

Pendleton, G. N., Briggs, M. S., & Meegan, C. A. 1996, Gamma-Ray Bursts, 3rd Huntsville Symposium, C. Kouveliotou, M. S. Briggs, & G. J. Fishman, New York: AIP, 877

Piran, T. 1994, Gamma-Ray Bursts, 2nd Huntsville Workshop, G. J. Fishman, J. J. Brainerd & K. Hurley, New York: AIP, 495

Preece, R. D., et al. 1996, ApJ, 473, 310

Press, W., Teukolsky, S., Vetterling, W., & Flannery, B. 1992, Numerical Recipes in FORTRAN, 2nd ed., New York: Cambridge University Press, 658

Rees, M. J., & Mészáros, P. 1992, MNRAS, 258, 41

Rees, M. J., & Mészáros, P. 1994, ApJ, 430, L93

Rybicki, G. B., & Lightman, A. P. 1979, Radiative Processes in Astrophysics, New York: Wiley, 221

Tavani, M. 1996, ApJ, 466, 768

Voges et al. 1982, ApJ, 263, 803

Fig. 1.— A comparison between the fitted values for β from two different spectral models (GRB & BPL) for 4B 950403.

Fig. 2.— A 2-D contour plot showing correlation between $E_{\rm peak}$ and β in the broken power-law model. A solid dot indicates the best-fit values for the two parameters. As discussed in the text, note that the 1σ contour on this figure is appropriate for only one parameter of interest, that is, it represents $\Delta\chi^2 = 1$, rather than 2.3, which would contain 68% of the *joint* probability. The data are from the interval 7.680 – 7.808 s of 4B 950403.

Fig. 3.— Histograms of the log. of the χ^2 probability that β is a constant (*dotted line*) or exhibits a linear trend (*solid line*) throughout each burst. The bursts that have probabilities consistent with zero (indicating rejection of the model) are not shown for either of the two distributions (34 and 20, respectively).

Fig. 4.— Histogram of the weighted average of β for the burst sample (*solid line*). Overplotted is the subset of bursts for which a constant value for β resulted in acceptable values for χ^2, at the 10^{-4} level of significance (*dotted line*).

Fig. 5.— Example of hard-to-soft spectral evolution in β for 3B 911118. Both the fitted value of β with their errors (*solid crosses*) and the burst count rate history (*dotted lines*) are plotted as a function of time.

Fig. 6.— Histograms for the distributions of coefficients of correlation between β and time (*solid line*) and $E_{\rm peak}$ (*dotted line*) for the burst sample.

Fig. 7.— Histogram of the total change in the high-energy power-law index (fitted value of $d\beta/d$t times the total time interval) for each burst in the sample. To improve the clarity of the figure, one outlier is not shown.

Fig. 8.— The fitted values of $E_{\rm peak}$ plotted against β for 3B 911118, illustrating correlation

between the time evolution of both hard and soft spectral components in a burst.

Fig. 9.— Example of positive correlation between fitted values of β divided by their linear trend ('detrended' β – *crosses*) and the time history of the count rate for 4B 9960924 (the count rate has been divided by the energy range $28 - 1800$ keV – *solid histogram*).